The base metal sulfide and Ni-Co arsenide-bearing veins of Valsassina (Lombardy, Italy): a preliminary study

Fabrizio Vergani[1], Marilena Moroni[2], Paolo Gentile[3], G. Diego Gatta[2]*

[1]Dipartimento di Scienze dell'Ambiente e della Terra "DISAT", Università degli Studi di Milano Bicocca, Piazza della Scienza 4, 26100 Milano

[2]Dipartimento di Scienze della Terra "A. Desio", Università degli Studi di Milano, Via Botticelli 23, 20133 Milano

[3]U.O. Piattaforma di Microscopia, Università degli Studi di Milano Bicocca, Piazza della Scienza 4, 26100 Milano

*Corresponding author: diego.gatta@unimi.it

1) Introduction

2) Geological background

2.1) Geological framework of Valsassina

2.2) The Valsassina hydrothermal system

3) Sampling and analytical methods

3.1) Optical and SEM petrographic observations

3.2) EPMA-WDS analyses

3.3) LA-ICP-MS analyses

3.4) C & O stable isotopes analyses

This is a 'preproof' accepted article for Mineralogical Magazine. This version may be subject to change during the production process.
DOI: 10.1180/mgm.2024.3

https://doi.org/10.1180/mgm.2024.3 Published online by Cambridge University Press

Abstract:

Valsassina (Lombardy, Northern Italy) is located in the Lombard southern Alps (Fig. 1). and is characterized by the presence of a metamorphic basement, by a major late-Variscan intrusive complex and by Carboniferous-Permian volcano-sedimentary cover units. These rocks host a pervasive system of poorly studied mineralized veins. These veins are characterized by base metal (Pb, Zn, Cu, Fe) and complex polymetallic assemblages. In this study, we have investigated various vein deposits in terms of ore textures, mineral chemistry of sulfides and sulfosalts (by EMPA-WDS and LA-ICP-MS analyses), stable isotopes (C and O) of carbonate gangue minerals, in order to have clues about the conditions of deposition of these ore deposits. Two different vein families can be recognized in Valsassina: NNW-SSE veins characterized by a complex polymetallic sulfide-sulfosalt assemblage, also with Ni-Co-Fe arsenides and other Ag-Bi-bearing minerals, and NE-SW veins with a simpler, base metal sulfide assemblage. The Ni-Co-bearing NNW-SSE veins show some distinctive features of the "five-element vein" type deposits, with the Ni-Co-Fe arsenide ore stage pre-dating a sulfide-tetrahedrite-dominated ore stage. LA-ICP-MS data on pyrite and sphalerite and stable isotopes (C and O) of the carbonate gangue minerals do not show clear differences between the two veins families, which are likely genetically linked. The isotopic compositions of the Valsassina vein carbonates are closely comparable with the signature of several major Five-element ore districts. Preliminary temperature estimates for the Valsassina vein systems were based on the sphalerite composition, applying the GGIMFis geothermometer. The estimated temperatures for the sulfide-dominated ore stage post-dating the Ni-Co minerals precipitation range between 100 and 250 °C. The crosscutting relationships observed for all the veins with the host rocks, suggest a possible late- to post-Variscan (late Permian) age, making these vein systems comparable with other late-post Variscan, polyphase hydrothermal events affecting large sectors of the Southern Alpine domain.

Keywords: Valsassina, ore deposits, base metal sulfides, Ni-Co arsenides, five-element veins, WDS, LA-ICP-MS, LA-ICPMS, C-O stable isotopes, pyrite, sphalerite.

https://doi.org/10.1180/mgm.2024.3 Published online by Cambridge University Press

1) Introduction

Located in the western end of the Orobic domain of the Southern Alpine belt (Lombardy, Northern Italy, Fig. 1), Valsassina represents a historically important mining area exploited since the Middle Ages (and probably before), especially for iron, lead, copper, silver and baryte. The valleys of Valsassina are host to various types of mineralization including Mississippi Valley-Type (MVT) deposits in Triassic limestone units (Rodeghiero et al., 1986; Vergani, 2022). There, swarms of hydrothermal veins comprising base metal (Pb, Zn, Cu, Fe) and complex polymetallic assemblages which occur in a variety of rock types ranging from Paleozoic metamorphic basement to Variscan intrusive rocks and Permo-Carboniferous volcano-sedimentary units.

None of these vein systems has previously been studied in detail, either in terms of geological setting, or mineralogical and geochemical features, although a spatial relationship with the Variscan Val Biandino intrusive complex (Di Colbertaldo, 1967; Crippa, 2017) may suggest a possible link to its hydrothermal circuit (Di Colbertaldo, 1967).

The Lombard Southern Alps host several late-Variscan ore deposits, mainly linked to magmatic-volcanic activities or to regional-scale hydrothermal systems. These deposits were exploited over the centuries, playing a key role in the Lombard economy which may extend to the present, as evidenced by the large unexploited U deposits of Novazza and Val Vedello (Cadel et al., 1986). Moreover, in the last few years, a series of new studies about the late-Variscan hydrothermalism of Lombard Southern Alps were published (*e.g.* Servida et al., 2010; Martin et al., 2017; Locchi et al., 2022; Zanchetta et al., 2022), underlining a renewed scientific interest in these deposits.

Based on preliminary observations (Bianchi, 1999; Vergani, 2019), this study represents a new contribution towards a thorough characterization of the vein-type ore deposits of the Valsassina district. Geological features of the mineralization are reported, along with the paragenetic reconstruction of the primary mineral assemblages based on data acquired using optical microscopy, electron microprobe analysis in wavelength-dispersion system (EMPA-WDS), laser ablation inductively coupled plasma-mass spectrometry (LA-ICP-MS) and stable isotope C-O analyses. The present investigations on the primary vein assemblages aim to provide a potential genetic model for this mineralization. ~~and to evaluate the possible relationships between these veins and the Val Biandino intrusion~~. Their characterization can eventually provide new insights for a better

https://doi.org/10.1180/mgm.2024.3 Published online by Cambridge University Press

understanding of the hydrothermal events which characterized the Southern Alps and their connection to the late-post Variscan geodynamic.

2) Geological background

2.1) Geological framework of Valsassina

Valsassina is located to the NE of the town of Lecco. Valsassina is bordered by the Grigna massif, to the West, and the margin of the Orobic Alps to the East.

The region is divided into two main structural domains by an important regional structure: the Valtorta Fault (see Fig. 2), a major transcurrent fault interpreted as being of Alpine age (Laubscher, 1985; Berra and Siletto, 2006). The northern domain consists of metamorphic rocks of the South-Alpine basement, the Val Biandino and Valle San Biagio intrusive complexes, Carboniferous to Permian volcano-sedimentary cover rocks, and finally Mesozoic carbonate rocks separated from the underlying Paleozoic rocks by the Northern Grigna thrust fault system (Fig. 2). The southern domain consists mainly of Mesozoic carbonate rocks.

The South-Alpine basement crops out in the core of a big regional fold structure, the Orobic Anticline. The basement consists predominantly of carboniferous paragneiss and quartz micaschists (315-350 M.y.), with rare kyanite relics, interpreted as products of a prograde Barrovian metamorphism, followed by retrocession to greenschist facies (Siletto et al., 1993). In the Orobic basement, metabasites and graphite schist levels also occur (De Sitter and De Sitter-Koomans, 1949; Cadel et al., 1996). In the Valsassina area, the Carboniferous-Permian volcano-sedimentary cover is represented by volcanic and continental clastic rock units of Monte Cabianca Fm., Pizzo del Diavolo Fm. and polymictic Ponteranica Conglomerate (Collio domain), followed by conglomerates and sandstones of the Verrucano Lombardo Formation that sealed, locally with angular unconformity, the complex stratigraphy of the Permian tectonic basins (Berra et al., 2016 and ref. therein). The intrusive complexes emplaced in the basement north of the Valtorta fault are the so-called Val Biandino quartz-diorite and the minor body of the Valle San Biagio Granite, the latter interpreted as a hypo-abyssal apophysis of the major Val Biandino intrusion (Crippa, 2017)(Fig. 2). The intrusive mass of Val Biandino emerges at the nucleus of the Orobic Anticline, precisely in the culmination of Valsassina and Valtorta Valley. The intrusion

https://doi.org/10.1180/mgm.2024.3 Published online by Cambridge University Press

is formed by two main stocks and by a series of lenticular masses and numerous leucogranitic, aplitic and pegmatitic bodies (Pasquarè, 1967; De Capitani, 1982; De Capitani and Liborio, 1988) (Fig. 2). The Val Biandino pluton is characterized by a pronounced lithological variability, with dominant biotite-bearing quartz-diorites (rich in mafic xenoliths) associated with tonalite and rarer gabbro-diorites and norites (*e.g.* one of the major lenticular outcrops north of Introbio). The pluton shows a calc-alkaline affinity, with a "bimodal" character of magmatism (De Capitani, 1982; De Capitani and Liborio, 1988). The Valle San Biagio Granite delimits the intrusive complex of Val Biandino to the West (Fig. 2). This intrusive body is composed of porphyritic leucogranites, occasionally with granophyric textures. The exposed contacts between the Valle San Biagio Granite and the Val Biandino plutons are always tectonic, underlined by tourmaline-bearing cataclasites (Sciunnach, 2001). In large sectors of Valsassina, the basement schists show widespread and sometimes extensive (up to 400 m-large) signs of thermo-metamorphism, suggesting that these intrusive bodies are largely sub-outcropping (see also Gaetani et al., 2012). A recent SHRIMP U-Pb study reported zircon age of 289 ± 0.8 Ma for the Val Biandino pluton and of 284.5 ± 1.0 for the Valle San Biagio Granite (Crippa, 2017). Therefore, the intrusion ages of Val Biandino and Valle San Biagio are coeval with the volcanic rocks of Monte Cabianca Fm. (Cadel, 1986), which may represent their effusive analogue (Froitzheim et al., 2008).

2.2) The Valsassina hydrothermal system

The hydrothermal vein deposits considered in this study occur in the central part of Valsassina. ~~and are spatially associated with lower Permian intrusive bodies emplaced within basement rocks.~~

The Valsassina vein deposits are hosted in a network of fractures with NE-SW/NNE-SSW and NNW-SSE orientations. Mineralization mostly occurs as vertical or sub-vertical lodes emplaced within metamorphic basement rocks and near the thermo-metamorphic contact halo of the Valbiandino intrusive (Di Colbertaldo, 1967). Some veins (*e.g.*, Prato San Pietro) crosscut the intrusive masses (Di Colbertaldo, 1967; Tizzoni, 1998), while others (*e.g.*, Camisolo, Fig. 2) intersect the local Permian volcano-sedimentary sequence.

The thickness of the veins ranges from a few meters up to over ten meters, with a strike extension that may reach over 1 km. The veins comprise mainly base metals sulfides such as galena, sphalerite, chalcopyrite and pyrite, along with minor arsenopyrite, bournonite and tetrahedrite, associated with quartz-baryte-carbonate gangue (Di Colbertaldo, 1967; Tizzoni, 1998; Bianchi, 1999)(Figs 3, 4). Ag-, Bi- and Ni-Co-bearing minerals

https://doi.org/10.1180/mgm.2024.3 Published online by Cambridge University Press

also occur in some deposits (Artini, 1903; Guastoni et. al., 2015; Guastoni et al. 2016a; Guastoni et al. 2016b; Bianchi, 1999)(Fig. 4).

The networks of faults that host the veins are considered as late-Paleozoic extensional fracture systems, preserved from subsequent reactivation during the Alpine orogeny (Sciunnach, 2001; Pohl et al., 2018) in analogy to what is observed in other parts of the Orobic basement to the East (*e.g.* Cadel et al., 1996).

3) Sampling and analytical methods

The Valsassina vein system was investigated at ten localities with ancient mine workings (Table 1): Camisolo, Cobio, Cortabbio (Sassi Rossi, Faidallo and Faedo mines), Valbona, Ceppo, Valle di Contra, Piattedo, Pra Piazzo, Val Rossiga and Valtorta (Frer and Costa Alta mines) (Figs 2, 3). Other five sites were preliminarily investigated only by the means of field inspections: Corno, Lombrega, Falpiano, Pessina-Valle delle Noci and Prato San Pietro mines. 43 samples were collected from mineralized outcrops exposed in trenches and open pits, accessible mine works and mine dumps (Fig. 3). The sampling strategy was planned on the basis of field observations. The sampling interested the most representative deposits, where specimens suitable for the petrographic observations and/or the analytical studies were collected. Samples for petrographic observations and preparation of polished sections for EMPA-WDS and LA-ICP-MS analyses were collected in the Valbona, Cortabbio and Camisolo mining areas (NNW-SSE veins), as well as in the Valle di Contra, Val Rossiga and Valtorta areas (NE-SW veins).

After mineralogical and microtextural characterization by optical microscopy, quantitative chemical microanalyses of major and accessory ore minerals were performed by EMPA-WDS and LA-ICP-MS. Ore petrography and microtextural observations were performed by optical and scanning electron microscopy on polished sections, obtained from selected samples from some of most representative veins. The same sections were then used for EMPA-WDS and LA-ICP-MS micro-chemical analyses on major and accessory ore minerals, along with additional micro-textural investigation.

A list of the studied localities and samples is in Table 1.

3.1) Optical and SEM petrographic observations

https://doi.org/10.1180/mgm.2024.3 Published online by Cambridge University Press

Representative samples taken from dumps, mineralized outcrops and accessible mining galleries were prepared for the reflected light optical microscopy and scanning electron microscopy (SEM) observations. The samples were initially embedded in a two-component epoxy resin (Araldite©) and subsequently cut and polished using silicon carbide grinding disks and 0.3-micron corundum dust.

The prepared samples were observed using a Zeiss Axioscope combined transmitted/reflected light optical microscope equipped with a digital camera. The use of the scanning electron microscope (SEM) with energy-dispersive X-ray spectroscopy (EDS) helped in identifying phases with uncertain attribution that could not be clearly distinguished through optical observations. SEM investigations were performed with a Tescan VEGA TS 5136XM equipped with an EDAX Genesis 4000 energy-dispersive system (EDS). The samples were positioned on aluminum stubs carrying bi-adhesive carbon pads and successively carbon coated (20 nm), in order to increase sample conductivity.

3.2) EMPA-WDS analyses

Quantitative chemical analyses in wavelength dispersive mode of tetrahedrite, Ni-Co arsenide/sulfarsenides, Bi-Pb sulfides and arsenopyrite were performed by means of a JEOL JXA – 8200 electron probe equipped with five wavelength-dispersive spectrometers at the Earth Sciences Dept. – Univ. Milan (ESD-MI). The analytical conditions for the electron beam were: accelerating voltage 15 kV, beam current 5 nA, beam diameter 1-2 μm, counting time for each element: 30 seconds on peak and 10 seconds on background. Elemental concentrations were determined after applying φ(ρz) algorithm and corrections for X-ray fluorescence, absorption, atomic number (Z) and matrix effects. Calibration for each element was done on the following standards, for which spectral lines, analyzing crystals and detection limits, in ppm, are given in brackets: Zn (pure Zn, Kα, LIFH, 650), Fe (fayalite, Kα, LIFH, 330), Cd (pure Cd, Lα, PET, 280), Cu (pure Cu, Kα, LIFH, 550), Ag (pure Ag, Lα, PET, 260), Ni (nickeline, Kα, LIFH, 350), Co (pure Co, Kα, LIFH, 350), Ge (pure Ge, Lα, TAP, 230), Pb (galena, Mα, PET, 450), Bi (pure Bi , Mα, PET, 330), Sb (pure Sb, Lα, TAP, 450), As (nickeline, Lα, TAP, 200) and S (pyrite, Kα, PET, 100). Backscattered electron (BSE) images were also collected.

Quantitative chemical WDS analyses on sphalerite and pyrite were performed by means of a Gemini 500 HR-FEG-SEM equipped with a Bruker parallel beam Quantax wavelength-dispersive spectrometer at the PMIB -

https://doi.org/10.1180/mgm.2024.3 Published online by Cambridge University Press

Milano Bicocca University. The analytical conditions for the electron beam were: accelerating voltage 15 kV, beam current 10 nA, beam diameter 1-2 µm, counting time for each element: 60 seconds on peak and 30 seconds on background. The same analyzed spots on sphalerite and pyrite were successively selected for the LA-ICP-MS analyses. Zn (Fe-bearing sphalerite standard, Lα line, TAP crystal, 500 ppm d.l.), Fe (pyrite standard, Lα line, BRML30 crystal, 400 ppm d.l.) and S (pyrite standard, Kα line, PET crystal, 500 ppm d.l.) were analyzed.

3.3) LA-ICP-MS analyses

LA-ICP-MS was used to analyze a wide range of trace elements in pyrite and sphalerite. Trace element analyses were carried out at the GeoRessources laboratory (Vandoeuvre-lès-Nancy, France), using a 193 nm MicroLas Pro ArF Excimer coupled with a Agilent 7900 quadrupole ICP-MS. Laser ablations were performed with a constant 5 Hz pulse rate, 60-micron spot size, at 6 J laser energy. The ablation duration for background, peaks and washouts was 30, 40 and 20 s, respectively. The integration time was 20 ms for all the elements. The ablated material was transported using a constant He flow (650 ml/min) and mixed with Ar in a cyclone coaxial mixer, prior to entering the ICP torch and being ionized. The ions were successively sampled, accelerated and focused before being separated and analyzed in the quadrupole mass spectrometer. The concentrations of the following isotopes were measured: ^{47}Ti, ^{51}V, ^{55}Mn, ^{57}Fe, ^{63}Cu, ^{66}Zn, ^{59}Co, ^{60}Ni, ^{71}Ga, ^{74}Ge, ^{75}As, ^{78}Se, ^{85}Rb, ^{88}Sr, ^{89}Y, ^{90}Zr, ^{93}Nb, ^{95}Mo, ^{107}Ag, ^{111}Cd, ^{115}In, ^{118}Sn, ^{121}Sb, ^{125}Te ^{133}Cs, ^{137}Ba, ^{139}La, ^{140}Ce, ^{141}Pr, ^{146}Nd, ^{147}Sm, ^{153}Eu, ^{157}Gd, ^{159}Tb, ^{163}Dy, ^{165}Ho, ^{166}Er, ^{169}Tm, ^{172}Yb, ^{175}Lu, ^{178}Hf, ^{181}Ta, ^{182}W, ^{197}Au, ^{201}Hg, ^{205}Tl, ^{208}Pb and ^{209}Bi. Mn, Cu, Co, Ni, Ag, Ga, Ge, Se, As, Sb, Mo, Cd, In, Sn, Y, REE and Bi were analyzed in sphalerite. V, Cu, Zn, Pb, Co, Ni, Ga, Ge, Se, Sb, As, Hg, Mo, Ag, Te, Au, Tl, Y, REE, Ti, Rb, Sr, Cs, Ba, Hf, Nb and Ta were analyzed in pyrite. The analyses were calibrated with MASS-1 and NIST610 standards. Iron and zinc concentrations of pyrite and sphalerite were used as internal standards respectively. Limit of detection (LOD) and uncertainty depends on the ablation spot diameter and the analyzed element. For each analysis, LOD was calculated using the 3σ criterion detailed in Longerich et al. (1996), uncertainty was calculated including the ones on the net transient signal (σ) and on the internal standard concentration. Minimum LOD were usually lower than 1 ppm for the trace elements analyzed at ablation 60 µm spot diameters (see Tables 1-2 ESM).

https://doi.org/10.1180/mgm.2024.3 Published online by Cambridge University Press

3.4) C & O stable isotopes analyses

Carbon and oxygen isotopic compositions of the carbonate-bearing samples from the Valsassina veins, coupled with carbonate reference materials, were measured at the ESD-MI. The equipment employed was a ThermoFisher Delta V Isotope Ratio Mass Spectrometer (IRMS), coupled with a Finnigan 2 gas bench. Powders were obtained from 13 carbonate-rich chips. Attempts were made to select carbonate fragments from sulfide-poor portions of the samples, in order to avoid analytical issues. Consequently, special care was taken to remove sulfide crystals, when present, before grinding. A mass of materials ranging between 0.25 mg (pure carbonates) and 0.7 mg (samples with variable fraction of quartz or silicates from wall rock) was used. Carbonate reference materials, *i.e.* international standards 603, NBS-18 and CO-8 and an internal reference MAMI (Carrara Marble), were employed for monitoring the efficiency of the system and the reproducibility of data. The standards employed were calcite of marine and magmatic origin, respectively. The additional reference materials were represented by hydrothermal mineral species similar to those occurring in the samples (siderite, ankerite) and previously analyzed by Cortecci and Frizzo (1993), and at the MLR Key Laboratory of Isotope Geology, Institute of Mineral Deposits in Beijing (China; see Martin et al., 2017). Powders of samples, international standards and internal reference samples were placed into borosilicate vials, sealed with butyl rubber septa, and flushed with CO_2 at 70°C for 5 minutes for extracting air. Subsequently, pure anhydrous phosphoric acid was added, and acidification of the powder was performed at 80°C for 12 hours, before the session of isotopic analysis. The high temperature coupled with the small amount of powder ensures a complete dissolution of refractory carbonates and the absence of fractionation due to incomplete reaction of refractory carbonate species before the isotopic analysis. The average $\delta^{18}O$ and $\delta^{13}C$ values for each sample were derived from a series of ten measurements. The $\delta^{18}O$ and $\delta^{13}C$ values are reported using the delta (δ) notation in *per mil* (‰), relative to Vienna Peedee belemnite (V-PDB) and Vienna standard mean ocean water (V-SMOW), respectively, with precisions of 0.06 to 0.2‰. Data normalization was performed according to the two-point method described in Paul et al. (2007) and comparing each "unknown" sample with both international standards and internal reference material affine to the samples.

https://doi.org/10.1180/mgm.2024.3 Published online by Cambridge University Press

4) Results

3.1) Field observations

~~Bibliographic information about the Valsassina ores is rather fragmentary, if non-existent, for many vein deposits. Therefore, this is the first attempt at an overall of building up an overall framework of the Valsassina ore district.~~

According to our field observations (Fig. 3), the Valsassina veins are characterized by two main end-member gangue assemblages, I) baryte-dominated and II) quartz-dominated, although a "mixed" quartz-carbonate-baryte assemblage is also recognized. Moreover, we found that the veins can be divided in two different families based on their directions (Fig. 2): a first set trending in an NNW-SSE direction, and a second set in a NE-SW direction. In fact, this difference in direction of the lodes appears to be also associated with some major differences in the vein fillings and in gangue and sulfide assemblages. The second vein set (NE-SW) is characterized by quartz-dominated or mixed gangue, while baryte-dominated gangue can be observed only in the first vein set (NNW-SSE, *e.g.* Cortabbio and Camisolo). Interestingly, in the baryte-dominated veins, the metallic minerals often occur as minor components of the vein filling, whereas the quartz-dominated and "mixed" gangue veins often display higher sulfide abundance coupled with a wide range of sulfide textures from semi-massive to disseminated (Fig. 4). In general, the veins are irregular, with stockwork/braided and "pinch-and-swell" geometries (with thickness often abruptly varying from over one meter to a few centimeters) or truncation by fault planes.

The NNW-SSE vein set (Cortabbio, Camisolo, Valbona and Cobbio lodes) is characterized by a complex mineralization, here indicated as "polymetallic", comprising galena, sphalerite, chalcopyrite, accompanied by significant fractions of tennantite-tetrahedrite, arsenopyrite and pyrite, along with bournonite and Ni-Co minerals. At Cortabbio, big masses of sulfides and Ni-Co minerals are always found at the footwall selvage of the baryte-dominated vein. In addition, we found some samples from the Valbona mine dumps containing a

https://doi.org/10.1180/mgm.2024.3 Published online by Cambridge University Press

peculiar arsenopyrite-pyrite-rich ore facies, which is unique for the area and has an unknown spatial relation to other paragenetic associations in these lodes.

The second NE-SW vein set (*i.e.,* Ceppo, Valle di Contra, Piattedo, Pra Piazzo, Corno, Lombrega, Falpiano, Valtorta, Val Rossiga and Prato San Pietro) is characterized by a simpler paragenesis, dominated by the presence of base metal sulfides like galena, sphalerite and chalcopyrite.

Further descriptions about our field observations of the macroscopic features of mineralization, textures, etc. are provided in the Electronic Supplementary Material (ESM).

4.2) Ore petrography

4.2.1) NNW-SSE trending veins ("polymetallic lodes")

In the Cortabbio, Camisolo and Valbona lodes, the ore phases are semi-massive, disseminated, brecciated and cement by gangue minerals. Sphalerite is usually mildly transparent, sometimes with irregular optical zoning marked by alternating areas (Fig. 5a), either rich in internal reflections or darker and less transparent. Sometimes, micro-inclusions of chalcopyrite, resembling chalcopyrite disease, are observed at the borders of sphalerite, which occasionally also includes relatively large amoeboidal tetrahedrite grains. Galena is observable as coarse-grained masses usually characterized by the presence of tetrahedrite blebs. Galena also commonly occurs as inclusions inside the other sulfides, mainly within sphalerite and chalcopyrite. At Valbona galena commonly occurs also as veinlets crosscutting coarse sphalerite grains. Chalcopyrite is often replaced by secondary covellite and goethite. Tetrahedrite is common as anhedral grains associated with the other sulfides, but it also occurs as stockwork veinlets (Camisolo lode) and as common blebby inclusions inside galena (Fig. 5b). At Camisolo tetrahedrite is sometimes fractured and cemented by a secondary mineral with dark greenish internal reflections (Fig. 5c). Pyrite occurs as coarse to fine grained euhedral crystals usually widespread in quartz gangue but also associated with galena, sphalerite and chalcopyrite. At Camisolo and Valbona mines pyrite can host tetrahedrite and galena blebs. Pyrite grains may also show Ni-Co sulfarsenide crystals in their cores. In general, pyrite seems to be the youngest among the most common sulfides. Moreover, at Cortabbio pyrite is also observed as inclusions with chalcopyrite or as coarse-grained aggregates overgrown by Bi sulfosalts and sometimes also with an evident internal zoning underlined by color variations. These

https://doi.org/10.1180/mgm.2024.3 Published online by Cambridge University Press

considerations seem to suggest the presence of two different pyrite generations within the Cortabbio ore. Arsenopyrite is particularly abundant in the Valbona mine, whereas it is an accessory mineral in the Cortabbio veins. In the Valbona mine arsenopyrite occurs as large, brecciated aggregates, locally associated with accessory bismuthinite, and interstitial to abundant subhedral pyrite grains affected by moderate fracturing (Fig. 5d). These brecciated aggregates are cemented by galena, sphalerite, tetrahedrite and gangue minerals of the main Valbona ore association. This arsenopyrite-pyrite ore facies seems to be older than the other sulfides of Valbona lode.

In the Cortabbio samples, two different ore assemblages were observed: a sulfide-rich and an arsenide-rich one. In the sulfide-rich assemblage, the main observed sulfide is chalcopyrite, coupled with abundant dissemination of tetrahedrite, pyrite, galena and Ni-Co sulfarsenides. Various Ag-Bi sulfides and sulfosalts (up to 100 µm in size) occur as poly-granular blebs and lamellar aggregates often intergrown with the sub-millimetric galena inclusions (up to 500 µm; Fig. 6a) in chalcopyrite (Fig. 5e); the whitish gray-blue, Bi-bearing phases are easily distinguished from galena and from each other by their variable degree of pleochroism and anisotropy. Blebs of Bi-bearing sulfosalts were also detected, such as aikinite and various undetermined phases. The quartz gangue is commonly disseminated with accessory small, white, euhedral, isotropic crystals (Fig. 5f), corresponding to zoned alloclasite-glaucodot (Co,Fe)AsS (see section 4.3.4), in association to rutile.

In the Cortabbio arsenide-rich samples (Fig. 5g-j), the assemblage is dominated by Co-bearing Ni arsenides with nodular to massive texture, in a gangue that consists of silicified host rock fragments and hydrothermal carbonates (euhedral, bladed siderite and subordinate dolomite). The Ni-Co nodules grow over discontinuous carbonate selvedges that pass laterally to micro-breccias with host schist fragments cemented by carbonates and accessory subhedral rutile. The cores of the arsenide nodules consist of rosettes of pink, pleochroic and strongly anisotropic nickeline (NiAs) with mosaic-like texture (Fig. 5h-i), radially overgrown by dense aggregates of white, pleochroic and anisotropic rammelsbergite lamellae ($NiAs_2$) and, less frequently, by fine-grained, grey-white, isotropic aggregates of Ni-Co sulfarsenides. The nickeline rosettes usually start growing over carbonate or quartz micro-fragments as seeds. The external surface of the Ni-Co nodules is characterized by finely zoned crusts and minute, often euhedral, crystals of Ni-Co sulfarsenides (Fig. 6b). Ni-Co

https://doi.org/10.1180/mgm.2024.3 Published online by Cambridge University Press

sulfarsenides overgrow both nickeline and rammelsbergite, but are also present as disseminated euhedral crystals, usually with a pyrite core, in the carbonate-quartz gangue. These disseminated crystals are sometimes overgrown by galena and Bi sulfosalts. Extremely fine-grained native bismuth occurs in the internal parts of the arsenide nodules, as inclusions and along micro-fractures in nickeline and rammelsbergite, and as interstitial, coarse-grained aggregates easily mistaken for gold blebs (Figs 5j, 6b-c). The nodular Ni-Co arsenide mineralization and related quartz-siderite gangue are affected by later baryte veining not easily discernible by optical microscopy but made evident by SEM imaging (Fig. 6d).

4.2.2) NE-SW trending veins (base metal sulfide-dominated orebodies)

In this base metal sulfide-dominated vein family, the most common sulfides are sphalerite, galena, chalcopyrite and pyrite. The ore phases are semi-massive, disseminated, brecciated and cement by gangue minerals, as observed for the NNW-SSE veins. Sphalerite is usually moderately transparent with red or brown internal reflections. Sphalerite commonly presents chalcopyrite micro-inclusions, arranged according to regular patterns similar to chalcopyrite disease (Fig. 5k). In general, the sphalerite from NE-SW veins is characterized by a more extensive presence of chalcopyrite micro inclusions compared to the sphalerite of the NNW-SSE veins. Galena shows similar textures in both the NNW-SSE and NE-SW veins; however, it is characterized by the absence of Bi-Ag sulfosalt inclusions, with only sporadic tetrahedrite blebs at the Pra Piazzo vein. At the Pra Piazzo vein tetrahedrite is also present as small anhedral masses associated with carbonate gangue. Chalcopyrite is often replaced by secondary covellite and goethite, as observed for the NNW-SSE veins. Chalcopyrite is generally not characterized by inclusions of other sulfides. Pyrite is present mainly as coarse to fine grained euhedral crystals in quartz gangue or associated to galena and sphalerite, sometimes with Ni-Co arsenide crystals as inclusions, in a similar way to what was observed for the NNW-SSE veins. At Valle di Contra pyrite can host galena inclusions.

Accessory minerals detected in the samples from the Valle di Contra, Corno, Val Rossiga and Valtorta mines, observed in this study, are represented by hematite and magnetite inclusions in sphalerite (Fig. 5l) and rare Ni-Co sulfarsenide crystals, disseminated in quartz gangue. Sporadic small arsenopyrite crystals in quartz gangue can be observed at Valle di Contra. The gangue consists predominantly of quartz with minor Fe-carbonate and

https://doi.org/10.1180/mgm.2024.3 Published online by Cambridge University Press

rare apatite in open space filling, although occasionally brecciated vein textures occur with silicified host rock fragments affected by fine-grained disseminations of chalcopyrite and/or pyrite.

A paragenetic scheme for the Valsassina veins is proposed in Fig. 7.

4.3) Mineral chemistry of sulfides and sulfosalts

4.3.1) Sphalerite

Sphalerite from the base-metal sulfide-dominating NE-SW vein system is here represented by the data from the Valle di Contra, Val Rossiga and Valtorta orebodies, while the data from the Valbona, Cortabbio and Camisolo orebody are representative for sphalerite from the complex, "polymetallic" mineralization of the NNW-SSE vein system.

The average trace element concentrations of Valsassina sphalerite are shown in Table 2 (see also Table 1 ESM for the complete datasheet).

Iron and cadmium are the main minor elements in sphalerite from all the considered mineralized veins (Fig. 8a-b). In all the orebodies, sphalerite tends to be rather Fe-poor (Fig. 8a), with Fe contents higher than 2.50 wt% only for the Valtorta, Camisolo veins and the base-metal Valle di Contra veins, in which sphalerite shows similar Fe contents ranging between 1.95 and 3.67 wt% (average at 2.85, 2.97 and 2.93 wt%, respectively; see Fig. 8a). The other veins (Cortabbio and Val Rossiga show similar Fe concentrations (Fig. 8a), ranging between 0.19 and 1.00 wt% (average at 0.63, 0.62 and 0.42 wt%, respectively). Fe shows a clear inverse correlation with Zn (Fig. 8a-b).

In all the sampled veins, sphalerite displays a complex composition involving a wide range of accessory components. Cadmium is always present in all the analyzed sphalerites, with contents varying from 1100 to over 5000 ppm. In particular, the Fe-poor sphalerites show slightly higher Cd contents (averages around 3300 ppm), with the exception of Valtorta sphalerite, that shows Cd concentrations similar to the Fe-richer sphalerite (average. around 2000 ppm). Cobalt shows variable contents and higher concentrations in the Fe-enriched sphalerites (average. 99.6 ppm compared to average. 1.12 ppm of Fe-poor sphalerites), however the sphalerite from Valtorta shows high Co concentrations coupled with low Fe values (average. 102.3 ppm, Fig. 8a). If compared to cobalt, nickel shows very low concentrations (4.9 ppm maximum, often below detection). The

https://doi.org/10.1180/mgm.2024.3 Published online by Cambridge University Press

Fe-enriched sphalerites from Valbona, Camisolo and Valle di Contra mines have higher concentrations of Mn, Cu and Ag, when compared to the Fe-poor sphalerites from Cortabbio, Val Rossiga and Valtorta veins (see Fig. 8a). Moreover, the sphalerite from Valtorta vein shows higher concentrations of In, Pb, As, Sb and Bi with also lower Ge concentrations (Fig. 8a), if compared to the other studied veins (see Fig. 8a and Tab. 2). In general, Ga and Ge concentration are correlated with Cu (Fig. 8c).

All the studied sphalerite samples are characterized by a direct correlation between Ag-Sb (Fig. 8d) and Cu-Sb (Fig. 8e). These correlations can suggest the presence of tetrahedrite microinclusions.

4.3.2) Pyrite

The dataset includes 60 LA-ICP-MS point analyses of pyrite crystals from the NNW-SSE and NE-SW veins and 10 analyses of crystals from the brecciated pyrite-arsenopyrite ore of the Valbona vein. Table 3 shows the average major and trace element concentrations of the Valsassina pyrite (see also table 2 ESM for the complete datasheet). Pyrite found as internal core of Ni-Co sulfarsenides is always too small and not suitable for LA-ICP-MS analyses.

Antimony, As, Cu, Pb, Ni and Zn are important trace elements within pyrite from the NNW/SSE and NE/SW veins and compared to the Valbona brecciated pyrite, where Co is dominant (Fig. 9).

Pyrite in the NNW-SSE veins shows higher Cu and Sb average values, 1835 ppm and 2277 ppm respectively, compared to NE-SW veins pyrite (892 ppm and 1529 ppm, respectively); on the contrary, the As values are similar for both the vein systems (1486 ppm for NNW-SSE veins pyrite and 1529 ppm for NE-SW veins pyrite). Cu, Sb and As are far less concentrated in the Valbona brecciated pyrite (Fig. 9), with average values of 0.42 ppm, 0.10 ppm and 18.95 ppm, respectively. However, the Val Rossiga pyrite is relatively lower in Cu, Zn, Pb, Ag and Sb if compared to the other pyrite crystals from NE-SW veins and the NNW-SSE veins (Tab. 3). Average values of 33.6 ppm Zn and 146.2 ppm Pb for pyrite crystals from the NNW-SSE veins, and 19.3 ppm Zn and 327.1 ppm Pb for the NE-SW veins, can be compared to the very low Zn and Pb contents (2.7 ppm Zn and 3.38 ppm Pb) for the Valbona brecciated pyrite. In spite of the low concentrations, in the Valbona pyrite Pb shows a direct correlation with Cu and Sb (Fig. 9a-b), suggesting the possible presence of occasional bournonite micro inclusions. Pyrites from the NNW-SSE and NE-SW veins also show a direct

https://doi.org/10.1180/mgm.2024.3 Published online by Cambridge University Press

correlation between Sb-Cu (Fig. 9c) and Sb-Ag (Fig. 9d), thereby suggesting the presence of a Cu-Zn-Ag-Sb-bearing phase (*e.g.* tetrahedrite) in these pyrites, coherently to what observed by the petrographic study.

Co and Ni are minor components in pyrite from all the studied deposits (Fig. 9e). The Ni concentration ranges from 8 to 142 ppm (average 66 ppm) for the NNW-SSE veins and from 2 to 275 wt ppm for the NE-SW veins (average 65 ppm). The NNW-SSE and NE-SW pyrites are slightly Ni-enriched compared to the Valbona brecciated pyrite, which show Ni values between 10 and 147 ppm (average 31 wt ppm). On the contrary, Valbona brecciated pyrite is Co-enriched (11-223 ppm, average 79 ppm), if compared to the NNW-SSE veins (15-8.90 ppm, average 2.50 ppm) and the NE-SW veins (0.003-81.58 ppm, average 5.30 ppm). Therefore, the Valbona brecciated pyrite shows higher Co/Ni ratios (between 0.69 and 5.34, average 3.21) if compared to the NNW-SSE veins (0.003-0.21, average 0.05) and the NE/SW veins (0.001-0.61, average 0.08).

All the studied pyrites are depleted in Se, largely under the detection limit and with concentrations that do not exceed 35 ppm. The studied pyrites are also Te, Au, Tl, Mo and V-poor, but the pyrites from the NNW-SSE and NE-SW veins are, in general, relatively more enriched in these elements compared to the Valbona brecciated pyrite.

4.3.3) Tetrahedrite

The major element compositional data of the tetrahedrite solid solution (s.s.) (Table 3a ESM) show remarkable differences between the tetrahedrites in the Valbona, Cortabbio and Camisolo veins. The Valbona tetrahedrite displays minimal arsenic content (<0.95 wt%), representing a near end-member tetrahedrite, and with Ag content from 2.91 to 2.97 wt%. In the tetrahedrite of the Camisolo lode, the Sb/As ratios vary from 4:1 to 7:1, indicating the occurrence of tetrahedrite with minor As contents (up to 4.97 wt%), with Ag contents varying between 1.14 and 1.45 wt%. The tetrahedrite s.s. of Cortabbio lode displays Sb/As ratios of 1:4, therefore tends towards the As end-member tennantite (As 16.08-16.70 wt%, Sb 4.44-5.41 wt%), with a narrow range of Ag concentration (between 3.12 and 3.42 wt%). In addition, significant differences are observed for Fe and Zn (Table 3a ESM). In the Camisolo and Valbona As-poor tetrahedrite, Zn is dominant over Fe, whereas the tennantite from Cortabbio is Fe-rich. The general chemical formula of tetrahedrite/tennantite, calculated on the basis of 13 S atoms per formula unit, are: $(Cu_{9.20\text{-}9.47}Fe_{0.29\text{-}0.39}Zn_{1.53\text{-}1.61}Ag_{0.17\text{-}0.21})(As_{0.43\text{-}1.11}Sb_{2.56\text{-}3.71})S_{13}$ for the Camisolo lode, $(Cu_{9.12\text{-}9.17}Fe_{0.83\text{-}0.89}Zn_{1.18\text{-}1.19}Ag_{0.46\text{-}0.47})(As_{0.14\text{-}0.21}\ Sb_{3.98\text{-}4.01})S_{13}$ for the Valbona lode and

https://doi.org/10.1180/mgm.2024.3 Published online by Cambridge University Press

$(Cu_{9.07\text{-}9.12}Fe_{1.13\text{-}1.17}\ Zn_{0.82\text{-}0.89}Ag_{0.43\text{-}0.47})(As_{3.24\text{-}3.34}Sb_{0.54\text{-}0.67})S_{13}$ for the Cortabbio mine. The EMPA-WDS analyses also indicated that the Valsassina tetrahedrites are rather poor in accessory elements, generally close to or below instrumental detection limits with the exception of Pb, likely due to contamination by host galena, and localized Ni enrichments (at Camisolo).

4.3.4) Ni-Co-Fe arsenides and sulfarsenides

Ni-Co-Fe sulfarsenides and Ni arsenides are well represented in the Cortabbio lodes; whereas, in the base metal-rich veins, Ni-Co sulfosalts are very subordinate and represented by rare sulfarsenide with gersdorffite composition, usually occurring as micro-inclusions in the cores of euhedral pyrite crystals disseminated in quartz gangue. Table 3b ESM shows the EMPA-WDS data for the Ni-Co phases observed in this study.

The Ni arsenides, which characterize only the Ni-Co-rich facies of the Cortabbio lode, are represented by nickeline (NiAs) and rammelsbergite ($NiAs_2$). Nickeline is basically pure, whereas rammelsbergite, associated with gersdorffite in the external portions of the nodules, shows some compositional variation, due to incorporation of Co replacing Ni (max 5.47 wt% Co). Rammelsbergite has a general chemical formula of $Ni_{0.84\text{-}1.00}Co_{0\text{-}0.19}As_2$, whereas nickeline is stoichiometrically pure.

Ni-Co-Fe sulfarsenides occur most frequently and are represented by phases with variable compositions, here listed in order of abundance: gersdorffite with or without Sb and Co (ullmannite and cobaltite components, respectively), alloclasite-cobaltite and glaucodot. The external sulfarsenide crusts of the Cortabbio Ni-Co-Fe nodules are mainly composed of gersdorffite. Gersdorffite shows variable compositions, with substitutions of Sb for As and of Co for Ni. In general, gersdorffite at Cortabbio is characterized by a variable ullmannite component due to irregular incorporation of Sb (up to 9.84 wt%). The general chemical formula of the Cortabbio gersdorffite, calculated on the basis of one S atom per formula unit, is: $(Ni_{0.63\text{-}0.97}Co_{0\text{-}0.23})(As_{0.81\text{-}1.03}Sb_{0\text{-}0.13})S$. However, the sulfarsenide crusts displayed also a less common phase with a Ni-rich cobaltite composition (with 19.01 wt% Co and 10.89 wt% Ni). Alloclasite and glaucodot are commonly present as small euhedral crystals disseminated in quartz gangue in the sulfide-rich ore association of Cortabbio. Alloclasite has Co and Fe contents ranging between 19.73 and 24.34 wt% and between 8.2 to 9.87 wt%, respectively (Table 3b ESM). In glaucodot, Co and Fe range between 9.58-15.64 wt% and 17.18-25.17 wt%, respectively. Both the mineral species also contain minor components like Ni and Cu, with up to 2.26 wt% Ni and up to

https://doi.org/10.1180/mgm.2024.3 Published online by Cambridge University Press

6.08 wt% Cu, the latter probably due to (sub-)micro-inclusions of common Cu phases like chalcopyrite or tetrahedrite. The general chemical formulae of the two minerals, calculated on the basis of one S atom per formula unit, are: $(Co_{0.68-0.70}Fe_{0.29-0.30}Ni_{0-0.07})As_{1.06-1.07}S$ for alloclasite and $(Fe_{0.55-0.74}Co_{0.29-0.41})As_{1.04-1.09}S$ for glaucodot.

4.3.5) Other sulfides and sulfosalts

Arsenopyrite is a major mineral phase only in the distinct brecciated arsenopyrite-pyrite ore facies in the Valbona lode and shows minimal compositional variability and As contents compatible with its association with pyrite (Tab. 3b ESM). In the Valbona mine, bismuthinite is present in the form of micrometric inclusions inside pyrite crystals, associated to arsenopyrite. Bismuthinite displays accessory contents of Pb (0.6 wt%), Sb (0.14 wt%) and Ag (0.04 wt%) (Tab. 3c ESM). As mentioned above, in the chalcopyrite-galena ore facies of the Cortabbio lode, various Ag-Bi sulfides and sulfosalts were observed (Tab. 3c ESM). Among those, aikinite is the most common. Aikinite, already reported by Guastoni et al. (2015) for the Cortabbio lode, is nearly stoichiometric, with formula $Pb_{0.95}Cu_{0.92}Bi_{1.01}S_3$. Matildite is the second most common Bi-bearing metallic mineral at Cortabbio and has a calculated formula $Ag_{0.99}Bi_{0.98}S_2$. Minor wittichenite (calculated formula $Cu_{3.05}Bi_{0.97}S_3$) and rare ourayite are associated with matildite. Only one, out of the rare micro-blebs of presumed ourayite, was suitable for EMPA-WDS analysis. The calculated formula for this sulfosalt is $Ag_{2.70}Cu_{0.27}Pb_{3.87}Bi_{4.95}S_{13}$, with a good agreement with-the ideal composition.

4.4) Carbon and oxygen isotope data in ore-related carbonates

The isotopic $\delta^{13}C$ and $\delta^{18}O$ composition of the gangue carbonates (siderite and dolomite), from polymetallic and base metal sulfide-rich vein systems, is reported in Table 4 ESM. Data are plotted in Fig. 10a-b. Polymetallic veins are represented by siderite-rich samples only (representing both Ni-Co-arsenide ore and sulfide-tetrahedrite assemblage), whereas base metal sulfide-rich veins are represented by samples where either siderite or dolomite are the dominant carbonate species. In the $\delta^{18}O$ (V-SMOW) ans $\delta^{13}C$ (V-PDB) diagram of Fig. 10a, most of the Valsassina data plot in an elliptic cloud characterized by moderately negative $\delta^{13}C$ values (with low variability: between -1 and -5 *per mil*), and by $\delta^{18}O$ spread over a slightly wider range (between +14 and +20 *per mil*). Only one sample plots at lower $\delta^{13}C$ values, at –8.5 *per mil*. Dolomite-

https://doi.org/10.1180/mgm.2024.3 Published online by Cambridge University Press

dominated samples tend to plot at relatively heavier $\delta^{13}C$ values, although their difference with siderite, both in terms of $\delta^{13}C$ and $\delta^{18}O$ signatures, is minor. Table 4 ESM also reports evaluation of the isotopic composition of the mineralizing fluids in equilibrium with the ore-related siderite and dolomite gangues (Fig. 11), analyzed by employing mineral-fluid fractionation equations in function of temperature for siderite and dolomite *vs.* water and CO_2, respectively by Zheng (1999; Equations 1 and 2) and by Golyshev et al. (1981; Equations 3 and 4).

[1] $1000\ ln\alpha_{\text{siderite-water}} = 4.23 \cdot 10^6/T^2 + (-4.58 \cdot 10^3/T) + 1.73$

[2] $1000\ ln\alpha_{\text{dolomite-water}} = 1000\ ln\alpha = 4.06 \cdot 10^6/T^2 + (-4.65 \cdot 10^3/T) + 1.71$

[3] $1000\ ln\alpha_{\text{siderite-CO2}} = 0.07707 \cdot 10^{18}/T^6 + (-5.8544 \cdot 10^{12}/T^4) + 31.81548 \cdot 10^9/T^3 + (-63.55559 \cdot 10^6/T^2) + 51.46659 \cdot 10^3/T - 12.36038$

[4] $1000\ ln\alpha_{\text{dolomite-CO2}} = 0.07579 \cdot 10^{18}/T^6 + (-5.76702 \cdot 10^{12}/T^4) + 31.37431 \cdot 10^9/T^3 + (-62.58142 \cdot 10^6/T^2) + 49.20807 \cdot 10^3/T - 11.39305$

where α represents the isotope fractionation and T is the temperature in °C. The calculation was performed using the *Web Stable Isotope Fractionation Calculator* by Beaudoin & Therrien (2009).

5) Discussion

~~Most of the hydrothermal veins in Valsassina may be preliminarily grouped into two different vein types or families, characterized by distinct structure (*e.g.* the NNW *vs.* the NE orientation of host fractures) and mineralogical features (regarding both the ore and gangue minerals). As absolute geochronology data are not available for the mineralization age, such distinction, along with the evaluation of the local geological setting, may lead to hypothesize whether these vein families can be ascribed to two different events or to one polyphasic event.~~

Petrography, compositional features of sphalerite, pyrite and associated phases, as well as stable isotope analyses on carbonates, were employed in order to highlight the differences or the analogies between the sulfide assemblages of the NNW (polymetallic) *vs.* the NE (base metal sulfide-rich) vein families, as well as to compare these ore deposits with similar ore systems.

5.1) Ore petrography and mineral chemistry of major and accessory phases

https://doi.org/10.1180/mgm.2024.3 Published online by Cambridge University Press

The petrographic features of the sulfide-rich assemblages of the two vein families are broadly similar, although the NE veins display a simpler, basic assemblage due to the dominant presence of sphalerite, while chalcopyrite, galena and pyrite are only rarely accompanied by accessory sulfides and sulfosalts (*e.g.* tetrahedrite and Ag-Bi-bearing phases). Pyrite, in particular, shows identical features in both the vein families. It is also important to consider that the pyrite grains from both the NE/SW and the NNW/SSE veins often contain Ni-Co sulfarsenides in their cores. In both vein families, sphalerite is characterized by the development of chalcopyrite disease-like texture, following more or less regular patterns. However, in some of the base metal sulfide-rich veins, this texture in sphalerite is much more intensely developed and micro-inclusions of magnetite and hematite occur together with the overwhelming inclusions of chalcopyrite. As previously reported, pyrite and sphalerite from both veins systems are probably characterized by the presence of micro inclusions of possible Ag-bearing tetrahedrite, as suggested by the LA-ICP-MS analyses. However, Ni-Co sulfarsenides, arsenopyrite, tetrahedrite and bournonite are present as accessory minerals also in the NE-SW vein family. Considering this, it seems that the NE-SW and NNW-SSE veins are not defined by distinct parageneses, but rather by varying relative abundances of the metallic minerals.

Sphalerite can host a wide range of minor and trace elements, according to patterns that are considered as sensitive to variations of depositional conditions (as widely reviewed in Cook et al., 2009). In our study, the sphalerite data for Cd, Mn, Ga, Ge, Ni, Se, Bi, As, Sn and Ag do not help in discriminating between the polymetallic vein family and the base sulfide-rich family, whereas Fe, Co and In display markedly different signatures for the various orebodies, although independently from assemblages and structural orientation, as shown in Fig. 8a. The higher Fe contents sharply distinguish the Valbona, Camisolo and Valle di Contra lodes from all the others (Fig. 8a-b). Cobalt also contributes to this discrimination: it occurs in sphalerite from all veins, but it is less markedly enriched in the Fe-poor sphalerite of the Cortabbio and Val Rossiga lodes. A possible explanation of such cobalt distribution may be compatible with the presence or absence of other phases (like arsenides) that preferentially incorporate Co, and sequester it from the fluid where sphalerite may subsequently crystallize. Indium displays low contents, often below 1 ppm, and an irregular distribution in both vein systems, although it tends to be particularly enriched (median over 50 ppm and up to 830 ppm) in the Valtorta mine (Fig. 8a). Antimony and Cu are more enriched in the Valtorta sphalerite, but this is probably

https://doi.org/10.1180/mgm.2024.3 Published online by Cambridge University Press

due to the presence of tetrahedrite-like inclusions; indeed, Sb-Cu and Sb-Ag show a clear direct correlation in Valsassina sphalerite.

Previous studies have shown that divalent cations, such as Mn, Cd, Co, Cd and Fe can directly replace Zn in the sphalerite structure (*e.g.* Cook et al., 2009a; Ye et al., 2011). However, Cook et al. (2012) and Belissont et al. (2014) also demonstrate incorporation of trivalent and tetravalent cations, such as Ga^{3+}, In^{3+} and probably Sn^{3+} or Sn^{4+}, coupled with the monovalent Cu and Ag. Gallium and Ge are always detected in the sphalerites from all veins with maximum contents around 340 ppm and 130 ppm, respectively. A positive correlation was observed between Cu and Ga in all the studied sphalerite samples, supporting the coupled substitution $2Zn^{2+} \leftrightarrow Cu^{+} + Ga^{3+}$. There is also a positive correlation between Cu and Ge (as well as between Cu and Ga+Ge) in all the analyzed sphalerite spots (Fig. 8d), suggesting the presence of the coupled substitution $2Cu^{+} + Ge^{4+} \leftrightarrow 3Zn^{2+}$ and could point to reducing conditions in the ore-forming fluids (Cook et al., 2009a; Ye et al., 2011; Belissont et al., 2014). However, in these veins the absence of pyrrhotite and the occurrence of baryte as common gangue mineral and of magnetite + hematite inclusions in sphalerite from the Valtorta and Rossiga samples are not compatible with markedly reducing conditions.

Besides sphalerite, pyrite in the Valsassina veins was analyzed in detail. Several studies were carried out in the past about the incorporation of accessory elements in pyrite. It was found that the trace element composition of pyrite, when considering elements such as Co, Ni, As, Sb, Se, Zn, Cu, Pb and Ag can contribute to the characterization of the genesis of hydrothermal ore deposits (Cook & Chryssoulis, 1990; Cook et al., 2009b; Deditius et al., 2009; Deditius et al., 2014; Genna & Gaboury, 2015; Large et al., 2009; Reich et al., 2005; Reich et al., 2013). Trace elements in pyrite can be usually divided into three different groups (*e.g.* Wang et al., 2018 and reference therein): (1) the first group includes elements that can enter the iron sulfides crystal structure due to substitution of iron, such as Co, Ni and Tl, or due to substitution of sulfur, like As, Se and Sb (these elements can be also hosted by micro or nanoinclusions); (2) the second group consists of elements, such as Cu, Zn, Pb, and Ag, usually hosted by inclusions of other sulfide minerals; (3) the third group is characterized by high field strength and lithophile elements (such as Zr, La, Th, U and Ba), which most likely are hosted as oxides or silicate inclusions in the iron sulfides.

Affine to iron, Co and Ni often display a similar geochemistry, moreover they did not change their concentrations during pyrite recrystallization and they can be easily incorporated into its crystal structure (*e.g.*

https://doi.org/10.1180/mgm.2024.3 Published online by Cambridge University Press

Large et al., 2009; Koglin et al., 2010). Because of this, the Co/Ni ratio of pyrite has been considered useful in discriminating pyrite of different origins (*e.g.* Price, 1972; Bralia et al., 1979). High Co and Ni concentrations and high Co/Ni ratios (Co/Ni > 1) in pyrite may suggest an origin ascribable to a hydrothermal regime (Bralia et al., 1979). On the contrary, pyrite associated to a sedimentary environment usually has low Co/Ni ratios (<1, Ni-dominated). Hydrothermal pyrite may also have Co/Ni ratios < 1, in which case it is necessary to consider, for example, geological and mineralogical features, along with the genetic type of ore deposit (Bralia et al. 1979), for an unambiguous distinction. ~~For example, high Ni concentration associated with low Co/Ni ratio, have been observed in pyrite formed in organic matter-rich environments (Dill and Kemper, 1990; Guy et al., 2010). Furthermore, more reducing conditions can lead to enhanced Ni concentration of pyrite (Dill and Kemper, 1990; Maslennikov et al., 2009; Scott et al., 2009; Guy et al., 2010).~~

The pyrites from the NNW-SSE and NE- SW veins have low content of Co and Ni (average. Ni 66 ppm and Co 3.99 ppm) with a Co/Ni ratio ranging from 0.001 to 0.61 (mean 0.05 and 0.08, for NNW-SSE and NE-SW veins, respectively). In a similar way, the Valbona brecciated pyrite has low content of Co and Ni (average. Ni 31.8 ppm and Co 78.6 ppm) but shows Co/Ni ratios ranging from 0.69 and 5.34 (average 3.21), far different from the ones observed for the other pyrites. In general, all the studied pyrite samples show Ni-Co contents and Co/Ni ratios far lower than what expected for porphyry Cu deposits and other magmatic-related ore deposits, suggesting the lack of dominant hydrothermal fluids firmly ascribable to magmatic activity.

According to recent studies (Rajabpour et al., 2017; Li et al., 2021), the As concentration in pyrite may reflect the proportion of meteoric to magmatic waters within the system, with meteoric or basinal water abundances positively correlating with pyrite As concentrations. On the contrary, mineralizing fluids with higher abundance of magmatic waters would tend to form pyrite with higher concentrations of Co and lower concentrations of As. The pyrites from Valsassina veins are characterized by high As concentrations, on average around 1500 ppm, while the Valbona brecciated pyrites show low As concentration (average 18 ppm). The pyrites from the NNW-SSE and NE-SW veins plot close to the As apex in a Co–Ni–As diagram (Fig. 12), indicating that this pyrite may have been formed from hydrothermal fluids with a major component derived from surficial, meteoric waters. Instead, the data of the Valbona brecciated pyrite are dispersed toward the Co apex across the magmatic-hydrothermal/epithermal field, thereby suggesting an origin from a different context or else a different fluid, possibly with a deep component (Fig. 12).

https://doi.org/10.1180/mgm.2024.3 Published online by Cambridge University Press

5.2) Estimation of the temperatures of ore formation

Variations in sphalerite composition can be used for thermo- and barometric evaluation (e.g., Kullerud, 1953), for geothermometry (Frenzel et al., 2016), for discriminating between different genetic settings (*e.g.* Qian, 1987; Schwartz, 2000) and for tracking changes in ore/fluid interaction in a given ore deposit (*e.g.* Gottesmann and Kampe, 2007; Gottesmann et al., 2009). In absence of fluid inclusion analyses, preliminary temperature estimates for the Valsassina vein systems might be based on the sphalerite composition. As previously mentioned, the analyses of the accessory elements of sphalerite can be used to evaluate the temperature of the orebodies. In particular, here we apply the GGIMFis geothermometer of Frenzel et al. (2016) which is based on sphalerite Ga, Ge, In, Mn and Fe contents. ~~Frenzel et al. (2016). The method by Frenzel et al. (2016) is based on the statistic evaluation, by means of principal component analysis, of a large dataset of sphalerite compositions (from bulk rock, microprobe and laser ablation analyses) from a large number of ore deposits worldwide and correlating those data with the homogenization temperatures of fluid inclusions. The sphalerite geothermometer relies on contents of Ga, Ge, In, Mn and Fe, which appear to be most sensitive to temperature.~~ Table 4 shows the estimated temperatures for the Valsassina orebodies. As shown in Table 4, the estimated temperature for all the veins lies in the range 135-192 °C. The estimated temperatures for the Camisolo, Valbona, Rossiga, and Valtorta veins (160-190 °C) are slightly higher than those obtained for the Cortabbio and Contra veins (130-140 °C). ~~The following temperatures were determined for the studied sphalerites: 160-168°C for Valbona, 136-137°C for Cortabbio, 175-188°C for Camisolo, 135-136°C for Contra, 161-170°C for Rossiga, and finally, 178-192°C for the Valtorta vein.~~ These data highlight another similarity between the two vein systems. In fact, they share quite similar temperature ranges, which are generally indicative of medium to low-temperature mineralization. To delve into more detail, in each of the two vein systems, sphalerite appears to be formed at relatively higher temperatures (up to 190 °C) as well as at lower temperatures (as low as 135 °C). These observations are consistent with both the minor textural and compositional differences observed in sphalerite from the different veins and the possible multiphase deposition of these veins. Furthermore, by utilizing the temperature data obtained from the GGIMFis geothermometer, in conjunction with sulfur concentrations measured using LA-ICP-MS in sphalerite, we were able to plot our data in a sulfur fugacity-temperature diagram (see Fig. 13, adapted from Einaudi et al., 2003). It is worth noting that sphalerite samples extracted from both the NW-SE and NE-SW vein systems exhibit similar sulfur fugacity values. These

https://doi.org/10.1180/mgm.2024.3 Published online by Cambridge University Press

values fall within the stability range of pyrite and chalcopyrite, consistent with the observed sulfide assemblages within these veins.

The ore in the Cortabbio lode (Faidallo mine) contains the silver-bismuth sulfide matildite, as exsolution lamellae inside galena, with a Widmanstätten-like texture (Fig. 6a). As proposed by Craig (1967), matildite presents a complete solid solution with galena at temperatures above 215 ± 15 °C, while at lower temperatures it exsolves as lamellae in galena. For this reason, matildite exsolutions, along with the record of Ag and Bi contents in galena, can be used as a geothermometer for evaluating temperature above, below or near 215 °C. In the Cortabbio lode, galena associated with the matildite lamellae always shows significant Bi and Ag contents (in wt% units). Considering the co-association of the Ag-Bi-bearing galena and the matildite exsolutions, we can expect that the temperature conditions for the sulfide-rich association of Cortabbio lode are around 215 +/-15 °C. It is worth noting that this estimate is higher compared to the GGIMFis sphalerite geothermometer temperature for the Cortabbio sulfide-rich stage. This observation suggests that galena and bismuth-bearing minerals may form at slightly higher temperatures if compared to the sphalerite-rich assemblage. At Cortabbio, the bismuth minerals represent some of the first precipitated sulfides at the end of the Co-Ni-rich stage. This observation might suggest a slight decrease in deposition temperatures during the sulfide-rich stage at Cortabbio.

Temperature estimations for the Valbona pyrite-arsenopyrite brecciated ore association was obtained by means of the so-called arsenopyrite geothermometer (Kretschmar and Scott, 1976; Sharp et al., 1985): the formation temperature of Valbona pyrite-arsenopyrite-rich ore ranges between 365 and 385 C° (see Fig. 3 ESM and Tab. ESM 3b). As discussed earlier, this distinctive arsenopyrite-rich association likely predates the other sulfides within the Valbona vein. Given this, it is conceivable that the arsenopyrite facies might be related to an older mineralization, subsequently tectonized by fault reactivation and overprinted by the Valsassina hydrothermal system. Alternatively, it could be related to an earlier, higher-temperature syn-tectonic facies of the Valbona vein.

5.3) The native metals/Ni-Co-Fe arsenides association of Cortabbio lode: Valsassina as a five-element vein system?

For the description of a possible genetic model of these veins, it is important to consider the occurrence of hydrothermal Ni-Co phases and, in particular, the (high) concentration of Ni-Co-Fe arsenides in the Cortabbio

https://doi.org/10.1180/mgm.2024.3 Published online by Cambridge University Press

ore. The Valsassina deposits show some of the distinctive features of the usually termed "five-element veins". In particular, the paragenetic scheme for the Cortabbio vein system is closely comparable with what is observed in mining districts for five-element veins worldwide (Fig. 7).

Generally, hydrothermal vein deposits with native Ag, As or Bi overgrown by a succession of Ni, Co and Fe arsenides, usually encapsulated by carbonate gangue minerals, are called five-element veins (for the Ag, As, Co, Ni and Bi elements association; Kissin, 1992). However, this nomenclature does not correctly describe all subtypes of this mineralization type, as some elements do not occur at some sites and/or elements like Sb and U may additionally occur in others, so that sub-types may be considered. Markl et al. (2016), for example, distinguished between native Ag/Bi-dominated, arsenide-dominated and native As-dominated five-element veins. The host rock composition is also very variable and includes sedimentary, metamorphic and igneous rocks, the latter with acid to ultramafic composition. Reported formation temperatures, for the contexts where five-element veins occur, range from ~150 to 450 °C, but usually cluster around 200 °C (Kissin, 1992; Staude et al., 2012 - and references therein). According to petrographic observations (*e.g.* Ramdohr, 1975; Kissin, 1992; Ahmed et al., 2009; Kreissl et al., 2018 and references therein), all the five-element veins can be classified into several (usually four) successive ore stages that may not be observable or accessible in all the sites: "Ore stage 1": sulfides older than native metals and arsenides; "Ore stage 2": native metals; "Ore stage 3": arsenides growing on native metals; "Ore stage 4": sulfides younger than native metals and arsenides. The arsenide stage ("ore stage 3") is always followed by base metal sulfides and sulfosalts like galena, chalcopyrite, sphalerite, tennantite-tetrahedrite, occasionally accompanied by bismuthinite, acanthite, proustite, pearceite, aikinite, pyrite and others ("ore stage 4"). The ore stage 4 is usually followed by a late-stage, characterized by gangue minerals precipitation, usually carbonates but also baryte in minor cases (Kissin, 1992). Based on textural evidence, Markl et al. (2016) assumed a rapid and continuous ore precipitation process in the stage 1, 2 and 3, presumably caused by far-from-equilibrium conditions and developing within small fluctuations of the temperature ranges observed among stages in all ore districts. Kissin (1988) suggested that the formation of five-element veins is linked to the circulation of basinal brines during extensional tectonics. Marshall et al. (1993) hypothesized that silver deposition is caused by a decrease of chlorine activity as a consequence of the mixing of silver-rich highly saline fluids with connate-meteoric fluids. Recently, Markl et al. (2016) suggested that the genesis of these deposits can be ascribed to the mixing

https://doi.org/10.1180/mgm.2024.3 Published online by Cambridge University Press

between hydrocarbons-bearing fluids and metal-rich hydrothermal fluids, which lead to the formation of the unusual ore textures and assemblages. For example, the hydrocarbon-rich fluids can be the effect of natural fracking phenomena: ejection of hydrocarbons or hydrocarbon-bearing fluids during the breaking up of rocks. Oxidation of methane leads to very reducing conditions of the mixed ore fluid, which facilitates the precipitation of the native metals and arsenides far-from-equilibrium. Moreover, the progressive oxidation of methane leads to precipitation of calcite and other carbonates instead of other gangue minerals like quartz, as a consequence of the dissolution of CO_2 and concomitant increase in HCO_3 activity. Successively, the native metals/Ni-Co minerals precipitation stops when the hydrothermal system retains its original equilibrium. When considering the Valsassina deposits, the Cortabbio vein system shows characteristics expected for arsenide-dominated five-element veins and displays features of the ore stages 2, 3 and 4, with both cockade-like textures of the Ni-Co-As enrichments as well as the sulfide-dominating ore stage 4 particularly well developed. Considering the petrographic features of the Cortabbio vein ore, the Ni-Co arsenides appear to predate the sulfide-rich assemblages. Considering the arsenides, the first precipitated phases are dominated by Ni and represented by mono-arsenide nickeline followed by Co-bearing diarsenide rammelsbergite, followed by Ni-Co sulfarsenides (Fig. 14). Native metals (bismuth, lead and antimony) occur as small inclusions inside the Ni-Co arsenides, The Ni-Co-Fe nodules are always associated with and/or encapsulated in carbonate gangue (mainly siderite and dolomite), therefore they appear mainly as floaters in the carbonate gangue, with no or only very limited contact with the host rock. As mentioned above, the subsequent As-bearing phases are represented by Ni-Co sulfarsenides, which record the progressive increase of both S and Co in the mineralizing fluid: Co-bearing gersdorffite and intermediate members of gersdorffite-cobaltite series crystallize, followed by alloclasite and glaucodot (Fig. 14). The latter sulfarsenides are common accessory phases in the Cortabbio samples, rich in sulfides and tetrahedrite, where also a bismuth imprint is well expressed.

In the five-element veins, the native elements are usually partly dissolved during or after the growth of the arsenides and sulfarsenides/antimonides, leaving behind empty holes rimmed by the arsenide minerals (Markl et al., 2016), usually filled up by carbonate gangue minerals. In the Cortabbio ore, the nickeline rosettes that represent the core of the Ni-Co-Fe nodules usually start growing from carbonate fragments. Moreover, the nickeline mosaic textures suggest that this mineral might have been grown at the expense of another phase (Fig. 5h-i). The gersdorffite-cobaltite crusts, in the external portions of the Ni-Co-Fe nodules, commonly

https://doi.org/10.1180/mgm.2024.3 Published online by Cambridge University Press

include extremely fine-grained, sub-micrometric segregations of native bismuth. This can suggest that the Ni-Co arsenide and sulfarsenide may have grown also after the native bismuth or other native metals. Therefore, the following mineral precipitation sequence can be inferred (see also Fig. 7): 1) native metals, 2) nickeline + rammelsbergite + gersdorffite-cobaltite, 3) alloclasite-glaucodot + Ag-Bi-Pb sulfide/sulfosalts (galena, aikinite, matildite, wittichenite, ourayite) + chalcopyrite, tennantite, sphalerite, pyrite, bournonite.

Cortabbio may not be the only arsenide-rich vein deposit of the Valsassina district. As a matter of fact, some preliminary inspections of the poorly accessible Camisolo vein deposit reveal many analogies with Cortabbio. Ni-rich skutterudite nodules were observed in quartz-carbonate veinlets inside hydrothermally altered host volcanics. Remarkably, various arsenates of Co, Ni, U, Bi and heavy REE are associated with this mineralization (Vergani, 2019; Vergani et al., 2020). In the polymetallic Valbona, rich in sphalerite and Ag-bearing tetrahedrite, and Cobio orebodies (NNW-SSE trending veins), the ore mineral assemblage is comparable with the sulfide-rich association observed at Cortabbio.

~~It is worth to note that~~ The estimated temperatures for the Valsassina vein deposits are fully comparable with the most characteristic temperature ranges measured by fluid inclusion analyses and reported in the relevant literature for the five-element vein districts.

The two different veins families are possibly genetically related and the base-metal-rich NE-SW veins might be the ore stage 4 of the five-elements hydrothermal circulation, as well as the sulfide-rich associations of NNW-SSE veins.

The brecciated pyrite-arsenopyrite-rich ore of the Valbona vein is likely ascribable to a previous hydrothermal event. At the moment, there is no direct or clear evidence of the connection of this ore with the other base metal sulfide veins, likely because of the poorly accessible old mine galleries, although there are remarkable similarities between the mineral assemblages (pyrite, chalcopyrite, presence of abundant As as well as accessory Bi phases). The temperature estimation (365-385 C°, Fig. 13) for this particular ore association obtained by means of the arsenopyrite geothermometer are higher than the ranges of temperature obtained with the GGIMFis geothermometer for the sulfide-rich stage of Valsassina veins. The Valbona pyrite-arsenopyrite brecciated ore is characterized also by different trace element concentrations and Co/Ni ratio if compared to the Valsassina NNW-SSE and NE-SW veins. Considering also the temperature range obtained for this brecciated ore, it is possible to hypothesize an origin somehow ascribed to the hydrothermal circuit of Val

https://doi.org/10.1180/mgm.2024.3 Published online by Cambridge University Press

Biandino intrusive or to the Permian volcanism. This particular mineralization might represent the ore stage 1 of the Valsassina hydrothermal system, although with the present data it is not currently possible to fully validate this hypothesis.

In some cases (*e.g.* Odenwald, Burisch et al., 2017), the five-element veins occur in spatial association with intrusive bodies, but several lines of evidence suggest that mineralization is unrelated to magmatism. In the case of the Valsassina veins, the timing of the supposed five-element vein system is uncertain although it may have developed after the emplacement of the Val Biandino-Valle San Biagio plutonic complex.

Five-element vein systems are also found in other areas of the Alps, such as Usseglio in Piedmont and Kaltenberg in Switzerland. The veins at Usseglio are hosted in an ophiolite setting within the Western Alpine belt. Within these veins, Ni-Co-Fe arsenides mineralization precipitated at temperatures around 170 °C, as indicated by fluid inclusion studies (Moroni et al., 2019a). Interestingly, this mineralization is not uniformly distributed within the vein system, similar to observations in Valsassina. In fact, Ni-Co-Fe minerals are predominantly found in specific veins, particularly in the eastern portion of the vein swarm. The larger ore lodes are characterized mainly by siderite, along with baryte, ankerite, and accessory sulfides. Four distinct ore stages have been identified: 1) siderite, 2) baryte, 3) Co–Ni–Fe arsenides, and finally, 4) sulfides (Moroni et al., 2019a). These veins are likely associated with a low-temperature post-orogenic (post-Alpine) hydrothermal circulation of basinal brines, along fractures linked to distensive tectonics (Moroni et al., 2019a).

Similar five-element veins are also found in Kaltenberg, Switzerland, within the metamorphic basement of the Western Alps, Penninic Domain (Kreissl et al., 2018). These veins exhibit a complex geology with two main hydrothermal events (233 ± 10 Ma and 188 ± 32 Ma), related to distensive tectonics during the breakup of the Meliata ocean and Alpine Tethys. These events are also associated with in-situ remobilization of ores that occurred during the Alpine Orogeny. In these veins, both Co-rich and Ni-Co-rich assemblages can be identified.

In comparison to the Usseglio and Kaltenberg deposits, the Valsassina veins are distinctly Ni-dominated, featuring arsenides and sulfarsenides such as rammelsbergite, nickeline, and gersdorffite, with only minor Co-bearing gersdorffite, cobaltite, and allocalsite-glaucodote. Additionally, arsenides like löllingite, safflorite, and skutterudite are nearly absent in the Valsassina veins, in contrast to what is observed at Usseglio and

https://doi.org/10.1180/mgm.2024.3 Published online by Cambridge University Press

Kaltenberg. In Valsassina, as well as in other Alpine five-element deposits like Usseglio and Kaltenberg, native Ag is not observable, and the native metals appear to be mainly represented by native Bi, with the addition of native As at Usseglio.

5.4) C-O isotopic signatures of carbonates and fluids

The carbon and oxygen isotope analyses of the carbonate gangue, from the polymetallic and the base metal sulfide veins, provide additional clues to the evaluation of Valsassina deposits. In Fig. 10a-b, additional data, included for comparison, are represented by the isotopic signatures of marine carbonates of Phanerozoic age, and of carbonates (siderite, dolomite, calcite) from several worldwide Ni-Co bearing, five-element-vein-type mining districts, *i.e.* Bou Azzer (Morocco; dolomite and calcite, Maacha et al., 2015), Odenwald (SW Germany; calcite, Burisch et al., 2017), Cobalt-Gowganda, Thunder Bay and Great Bear Lake (Canada; Robinson and Badham, 1974, Changkakoti et al., 1986; Kerrich et al., 1986; Kissin, 1992) as well as the Ni-Co-rich Arburese vein system in SW Sardinia (Moroni et al., 2019b). The background also includes symbols for the isotopic data of sulfide-bearing siderite-bearing late-post-Variscan hydrothermal deposits in the Southern Alps (Cortecci and Frizzo, 1993; Martin et al., 2017), as well as the data from the Variscan syn-orogenic siderite veins of the Siegerland district, Rhenish Massif (Hein, 1993), for which crosscutting relationships with syn-late-orogenic Co-Ni mineralization were recently recognized (Hellmann et al., 2012). In the diagram of Fig. 10b, the range of $\delta^{13}C$ values of the Valsassina veins are further plotted together with additional literature dataset from reference five element vein-type districts worldwide, as Schwarzwald (SW Germany, Staude et al., 2007), Kongsberg (Norway; Segalstad et al., 1986; Kissin, 1992) and Great Bear Lake (Canada), with the distinction between isotopic signatures of ore-related dolomite and calcite. The data cloud obtained for the Valsassina veins reveals similarities between (1) carbonates of the Ni-Co-rich polymetallic veins and of the Ni-Co-poor base metal sulfide veins, and (2) the isotopic signatures of the siderite- and the dolomite-dominated samples. The reference data plotted in Fig. 10a for various worldwide five-element- vein-type ore districts represent isotope signatures of different carbonates (dolomite, calcite, siderite) and, sometimes, of different ore stages. The patterns of such reference data appear to be quite variable and, at least in some cases, they reflect fluid evolution or fluctuations in physical-chemical parameters during multistage ore deposition. However, at least one feature is common to all ore districts, as well as to the Valsassina data

https://doi.org/10.1180/mgm.2024.3 Published online by Cambridge University Press

cloud: the mildly to moderately negative $\delta^{13}C$ signatures of ore-related carbonates. There is a large variability in $\delta^{13}C$ values in several ore districts, although there is a compositional range of overlap encompassing the $\delta^{13}C$ range of the Valsassina veins (Fig. 10a-b). The rather restricted Valsassina cloud overlaps the compositional fields of the Great Bear Lake ores, of the Sardinian Arburese veins and the narrow field of the ophiolite-hosted Bou Azzer district. There is also similarity between the Valsassina signatures and those belonging to the other Southern Alpine siderite-sulfide ores. The similarity between dolomite and siderite signatures for both carbon and oxygen appears to be a distinctive feature of the Valsassina veins. The overall range of variation in $\delta^{18}O$ of the Valsassina cloud (from +13.6 to +18.5 *per mil*) is rather pronounced but it derives from the overlap between the siderite and dolomite compositions (Table 4 ESM). In the Variscan Siegerland siderite veins, Hein (1993) correlated the $\delta^{18}O$ data systematically with variations in trapping temperatures from fluid inclusion analyses (see Fig. 10a). ~~This might also be the case for the Valsassina veins, because of the variability in their estimated temperatures derived from the sphalerite geothermometer, suggesting conditions of mineral deposition within a thermal range of 138-180°C. In reference to this temperature interval, an evaluation was done of the isotopic composition of the fluids in equilibrium with both siderite and dolomite through experimentally determined mineral-water and CO_2 fractionation equations (Zheng et al., 1999; Golyshev et al., 1981; Ohmoto & Rye, 1979) (Table 4 ESM). The results suggest that siderite- and the dolomite-bearing ores might have crystallized from broadly similar fluids. The $\delta^{18}O$ signatures of both fluids cluster within the narrow range of 3.7÷5.9 per mil (at 180°C), although the carbon of the siderite-related fluid is isotopically lighter ($\delta^{13}C$ fluid between -7 and -9 per mil at 180°C) than that in dolomite-related fluid ($\delta^{13}C$ fluid -4.5 per mil at 180°C). Both the Valsassina $\delta^{18}O$ and $\delta^{13}C$ fluid signatures are close to the restricted ranges of magmatic water and igneous carbon reservoir ($\delta^{18}O = 6 \div 10$ per mil; $\delta^{13}C = -4 \div -7$ per mil; Hoefs, 2009), although the lighter $\delta^{13}C$ fluid values for the siderite samples might suggest some interaction with organic carbon-bearing rocks. The latter feature is in common with several Ni-Co arsenide-bearing hydrothermal systems mentioned above. The moderate isotopic differences inferred for the ore-related fluids at Valsassina might either suggest the occurrence of distinct hydrothermal cells along the vein systems or mark different depositional stages, in agreement with the polyphasic nature of the mineralization.~~

An evaluation was done of the oxygen isotopic composition of the fluids in equilibrium with both siderite and dolomite through experimentally determined mineral-water fractionation equations by Zheng (1999) (see

https://doi.org/10.1180/mgm.2024.3 Published online by Cambridge University Press

section 4.4). Fig. 11a-b displays the plots of the $\delta^{18}O$ composition of fluids in equilibrium with siderite and dolomite belonging to the different assemblages (*i.e.*, polymetallic and base-metal veins) *vs.* temperature, according to the method in Mondillo et al. (2018). The mineral-fluid fractionation curves for Valsassina siderite and dolomite form bundles displaying moderate overlap across the whole temperature interval shown, from 0° to 400°C (Fig. 11a). However, the plot of the arithmetic averages of the fractionation curves for each group (Fig. 11b) allows us to observe an intersection between the dolomite fractionation curve and the one related to siderite from polymetallic veins. The low-angle intersection involves a wide temperature interval, spanning approximately from 50° to 125°C; however, the upper range of such interval is compatible with the lower temperature estimates obtained by means of the sphalerite geothermometer for polymetallic veins (130-140°C; see Section 5.2 and Fig.13).

Besides confirming the overall isotopic coherence among the Valsassina hydrothermal veins, such findings suggest that the dolomite-bearing base-metal veins, poorly exposed in some of the old Valsassina mining sites, might be related to the main mineralized system represented by the polymetallic veins and represent peripheral portions of such system.

For the siderite veins for which a thermometric estimate from sphalerite is available (Cortabbio, Valbona, Valtorta and Rossiga), it was possible to estimate the $\delta^{13}C$ composition of the fluid in equilibrium with siderite, for the temperature ranges of 130-140° and 160-190°C, *via* the equation by Golyshev et al. (1981) (see section 4.4). The corresponding equation for dolomite-fluid fractionation by Golyshev et al. (1981) was employed to estimate the isotopic $\delta^{13}C$ signature of the fluid in equilibrium with the average dolomite $\delta^{13}C$ composition at 120-130°C, *i.e.,* near the upper limit of the overlap between the fluid fractionation curves for siderite and dolomite in Fig. 11b. All fluid $\delta^{13}C$ signatures for siderite and dolomite are negative, between -6.8 and -13 *per mil* (see Table 4 ESM), only marginally intersecting the restricted range of igneous carbon reservoir ($\delta^{13}C$ = -4 ÷ -7 *per mil*; Hoefs, 2009). These results suggest that the siderite- and dolomite-bearing ores might have crystallized from broadly similar fluids, although the lighter $\delta^{13}C$ fluid values, recorded in siderite samples, might be the result of interaction with organic carbon-bearing rocks.

5.5) Age and metal sources

https://doi.org/10.1180/mgm.2024.3 Published online by Cambridge University Press

Direct intersections between the base metal and five-element/polymetallic veins are not observable, neither in the accessible mining works nor in the outcrops. The most recent information available for the fault systems that host the orebodies is restricted to the work by Pohl et al. (2018, and references therein), who support the early Permian age of some of the structures in relation to N-S extensional tectonics, and a modest reactivation during the Alpine orogeny. Geochronological data of the mineralized bodies in Valsassina are currently not available; however, a late-post-Variscan age may be viable in response to the observed crosscutting relationships and the evaluations by Pohl et al. (2018). In fact, these veins crosscut the Valsassina plutons and are truncated by the erosional unconformity at base of the Verrucano Lombardo Fm. (Bianchi, 1999), suggesting a vein emplacement between Lower and Upper Permian. This age estimation would be comparable also with the time span of the regional-scale siderite ± polymetallic sulfide mineralization affecting large sectors of the Southern Alpine domain (Martin et al., 2017). These siderite ± sulfide veins are also evident in Valsassina, and are also frequently found not far from the areas characterized by the sulfide veins discussed in this study. The genesis of the siderite ± sulfide veins is probably linked to a hydrothermal circulation of iron-rich fluids during the Permian to Early Triassic period, characterized by groundwater originating from meteoric freshwater (with also a marine contribution during Early Triassic) infiltrated along syn-depositional faults, heated up to 250°C at depths of 1000–2000 meters by the high geothermal gradient due to the Permian magmatism. In these veins, minerals like galena and sphalerite are usually present as accessory sulfides, which, in contrast, dominate in the Valsassina veins. The sulfide associations in the Valsassina veins are notably more similar to those documented in the quartz breccias of the Gromo-Gandellino area, characterized by galena, sphalerite, chalcopyrite, pyrite, arsenopyrite and tetrahedrite (Servida et al., 2010). The genesis of these quartz-sulfide breccias is connected to a hydrothermal circuit connected to volcano-phreatic activity; in fact, the breccia bodies can be the product of early phreato-magmatic activity related to the volcanism of the Collio Basin (Servida et al., 2010). In both the sulfide-bearing breccias and the siderite ± sulfide veins, Ni-Co sulfarsenides can be recognized as accessory phases, although the occurrence of Ni-Co mineralization affine to five-element vein-type deposits makes the Valsassina vein system different from the other late-Variscan Southern Alpine hydrothermal systems.

As previously discussed, the arsenide-free and likely granite-related pyrite-arsenopyrite-rich brecciated Valbona mineralization might be considered as a potential “ore stage 1”. If so, the local magmatic rocks may

https://doi.org/10.1180/mgm.2024.3 Published online by Cambridge University Press

have played a role on the presence of Ni and Co in the five-element vein mineralization. Ni and Co in these veins might have been leached by the hydrothermal fluids from the basic portions of the Val Biandino intrusive complex, or from the amphibolite horizons widespread in the Orobic basement (Cadel et al., 1996; De Sitter and De Sitter-Koomans, 1949). However, the potential of mafic rocks alone for Co mineralization has been recently discussed by Konnunaho et al. (2018), who envisaged the necessity of contamination processes of mafic rocks, especially through post-magmatic hydrothermal alteration and pre-enrichment of metals, in particular Co, by influx of CO_2-rich saline fluids. These saline fluids are not far from those considered in the model outlined by Kissin (1988; 1992), who suggested that the formation of five-element veins is caused by the circulation of connate brines ("basinal brines") in environments of continental rifting, *i.e.,* in the same tectonic regime that characterized the southern Alps during Permian-Early Triassic. On the other hand, considering instead the model proposed by Markl et al. (2016), the Valsassina veins might be the effect of the small-scale interaction between hydrocarbon-rich fluids and a pre-existing hydrothermal system, likely not too dissimilar from those already described in other areas of Southern Alps associated with late-post Variscan tectonic-magmatic activity. The hydrocarbon sources can be ascribed to the graphite schist and black-shales levels in the metamorphic basement and in the Collio Fm., respectively.

No data are available for the fluids responsible of the extensive vein system developed in Valsassina. In this light, it is currently not possible to correlate the veins to a plumbing system alimented by basinal brines, like those recorded in the other five element vein-type deposits or to interaction with hydrocarbon-rich fluids.

6) Conclusions

The sulfide veins in the Valsassina region have not received comprehensive study in the past, with research being largely fragmented. The present work constitutes the initial effort to provide a more detailed overview of these sulfide-bearing veins. However, due to challenges in sampling arising from the bad status of old mining works and the lack of supplementary data such as fluid inclusion studies, it is essential to regard this work as preliminary. Nevertheless, it has enabled us to gain a more in-depth understanding of these veins, which exhibits characteristics typical of five-element veins, especially in the case of the Cortabbio lode. Field studies and petrographic observations have unveiled the presence of two distinct vein families. The first is polymetallic and NNW-SSE oriented, while the second is NE-SW oriented and primarily characterized by base metal sulfides, with sulfosalts and nickel-cobalt sulfoarsenides present as accessory phases. Petrographic

https://doi.org/10.1180/mgm.2024.3 Published online by Cambridge University Press

analysis did not reveal significant differences in ore mineral textures between the two veins families. Instead, the distinction between the two vein families seems to be primarily based on the different relative concentrations of metallic minerals. In a similar way, trace element studies of pyrite did not show substantial differences between the two vein families. In contrast, trace element studies of sphalerite indicated some variations in elements such as indium and iron. These differences are also reflected in the slightly different temperature estimates obtained using the Frenzel et al. (2017) geothermometer for the studied veins. The C-O stable isotopes data obtained for the Valsassina veins reveals similarities between carbonates of the Ni-Co-rich polymetallic veins and of the Ni-Co-poor base metal sulfide veins, as well as the isotopic signatures of the siderite- and the dolomite-dominated samples. ~~In particular, the Valsassina data cloud overlaps the compositional fields of various world-wide five-element vein systems, such as the Great Bear Lake deposits, the Sardinian Arburese veins and the ophiolite-hosted Bou-Azzer district.~~

Based on the data obtained, it is conceivable that the NNW-SSE veins may represent ore-stage 4 of the five-element system. The NE-SW veins could be associated with either stage 4 or, alternatively, might represent ore-stage 1 of the five-element system. As of now, direct intersections between the base metal and five-element/polymetallic veins have not been observed, neither in accessible mining operations nor in outcrops. Therefore, the relationship between the two vein systems remains unclear, and the current data does not allow us to validate either of these hypotheses.

Geochronological data of the mineralized bodies in Valsassina are currently not available, however a late-post-Variscan age may be viable in response to the observed crosscutting relationships and the evaluations by Pohl et al. (2018). This age estimation would be comparable also with the time span of the regional-scale siderite ± polymetallic sulfide mineralization affecting large sectors of the Southern Alpine domain (Martin et al., 2017), although the occurrence of Ni-Co mineralization, affine to five-element vein-type deposits, distinguishes the Valsassina vein system from the other Southern Alpine siderite-sulfide vein systems.

Acknowledgements

G. Diego Gatta and Marilena Moroni acknowledge the support of the Italian Ministry of Education (MUR) through the projects "*Dipartimenti di Eccellenza 2023-2027*" and "*PRIN2017 - Mineral reactivity, a key to*

https://doi.org/10.1180/mgm.2024.3 Published online by Cambridge University Press

understand large-scale processes" (2017-L83S77). The authors are indebted with Dr. Elena Ferrari for the assistance during the stable isotope analyses and to Mr. Fabio Marchesini and Mr. Andrea Risplendente in samples preparation and assistance for the EMPA-WDS analysis. Fabrizio Vergani is grateful to Luigi Possenti and Giancarlo Valsecchi, mineral collectors and great connoisseurs of the mining history of Valsassina, for the information on the studied localities and for various samples, and to Massimiliano Stucchi, Andrea Gnata and Monica Corti for the help during the field works. The Editors and two anonymous Reviewers are thanked for the revision of the manuscript. This manuscript is dedicated to the memory of our friend and colleague Dr. Alessandro Guastoni, who worked extensively in Valsassina.

Competing interests

The authors declare none

References

Ahmed A.H., Arai S. and Ikenne M. (2009) Mineralogy and Paragenesis of the Co-Ni Arsenide Ores of Bou Azzer, Anti-Atlas, Morocco. *Economic Geology,* **104**, 249–266.

Artini E. (1903) Note mineralogiche sulla Valsassina. *Atti della Società Italiana di Scienze Naturali,* **42**, 1-19.

Beaudoin G. and Therrien P. (2009) The updated web stable isotope fractionation calculator. Pp. 1120-1122 in: *Handbook of stable isotope analytical techniques* (P.A. De Groot, editor). Elsevier, Netherland.

Belissont R., Boiron M.C., Luais B. and Cathelineau M. (2014) LA-ICPMS analyses of minor and trace elements and bulk Ge isotopes in zoned Ge-rich sphalerites from the Noailhac–Saint-Salvy deposit (France): Insights into incorporation mechanisms and ore deposition processes. *Geochimica and Cosmochimica Acta*, **126**, 518-540.

Berra F. and Siletto G.B. (2006) Controllo litologico e stratigrafico sull'assetto strutturale delle Alpi meridionali lombarde: il ruolo degli orizzonti di scollamento. *Rendiconti della Società Geologica Italiana Nuova Serie*, **1**, 1-3.

https://doi.org/10.1180/mgm.2024.3 Published online by Cambridge University Press

Berra F., Felletti F. and Tessarollo A. (2016) Stratigraphic Architecture of a Transtensional Continental Basin in Low-Latitude Semiarid Conditions: The Permian Succession of the Central Orobic Basin (Southern Alps, Italy). *Journal of Sedimentary Research*, **86**, 408-429.

Bianchi A. (1999) *Mineralizzazioni a barite e solfuri di Pb, Zn, Cu, Fe e Ag nel basamento cristallino della media Valsassina (LC).* Master thesis dissertation, University of Milan, Italy.

Bralia A., Sabatini G. and Troja F. (1979) A revaluation of the Co/Ni ratio in pyrite as geochemical tool in ore genesis problems. *Mineralium Deposita*, **14**, 353–374.

Burisch M., Gerdes A., Walter B. F., Neumann U., Fettel M. and Markl G. (2017) Methane and the origin of five-element veins: Mineralogy, age, fluid inclusion chemistry and ore forming processes in the Odenwald, SW Germany. *Ore Geology Reviews*, **81**, 42-61.

Cadel G. (1986) Geology and uranium mineralization of the Collio Basin (central Southern Alps, Italy). *Uranium*, 215-240.

Cadel G., Cosi M., Pennacchioni G. and Spalla M.I. (1996) A new map of the Permo-Carboniferous cover and Variscan metamorphic basement in the central Orobic Alps, southern Alps, Italy: structural and stratigraphical data. *Memorie di Scienze Geologiche*, **48**, 1-53.

Carothers W.W., Adami L.H. and Rosenbauer R.J. (1988) Experimental oxygen isotope fractionation between siderite-water and phosphoric acid liberated CO_2-siderite. *Geochimica et Cosmochimica Acta*, **52**, 2445-2450.

Changkakoti A., Morton R. D., Gray J. and Yonge C. J. (1986) Oxygen, hydrogen, and carbon isotopic studies of the Great Bear Lake silver deposits, Northwest Territories. *Canadian Journal of Earth Sciences*, **23**, 1463-1469.

Cook N.J. and Chryssoulis S.L. (1990) Concentrations of "invisible gold" in the common sulfides. *Canadian Mineralogist*, **28**, 1-16.

Cook N.J., Ciobanu C. L, Pring A., Skinner W., Shimizu M., Danyushevsky L., Saini-Eidukat B. and Melcher F. (2009a) Trace and minor elements in sphalerite: A LA-ICPMS study. *Geochimica et Cosmochimica Acta,* **73**, 4761–4791.

https://doi.org/10.1180/mgm.2024.3 Published online by Cambridge University Press

Cook N.J., Ciobanu C.L. and Mao J. (2009b) Textural control on gold distribution in As-free pyrite from the Dongping, Huangtuliang and Hougou gold deposits, North China Craton (Hebei Province, China). *Chemical Geology*, **264**, 101-121.

Cook N.J., Ciobanu C.L., Brugger J., Etschmann B., Howard D.L., De Jonge M.D., Ryan C.and Paterson D. (2012) Determination of the oxidation state of Cu in substituted Cu-In-Fe-bearing sphalerite via μXANES spectroscopy. *American Mineralogist,* **97**, 476-479.

Cortecci G. and Frizzo P. (1993) Origin of siderite deposits from the Lombardy Valleys, northern Italy: a carbon, oxygen and strontium isotope study. *Chemical Geology*, **105**, 293-303.

Craig J.R. (1967) Phase relations and mineral assemblages in the Ag-Bi-Pb-S system. *Mineralium Deposita*, **1**, 278–306.

Crespo M. T., Delgado A., Vindel Catena E., Lopez Garcia J.A. and Fabre C. (2002) The latest Post-Variscan fluids in the Spanish Central System: evidence from fluid inclusion and stable isotope data. *Marine and Petroleum Geology*, **19**, 323-337.

Crippa C. (2017) *Relazione tra il magmatismo Permiano e le strutture estensionali: caso di studio del Plutone della Val Biandino (Valsassina, LC).* Master thesis dissertation, Milano Bicocca University, Italy.

Curioni G. (1877) *Geologia applicata delle provincie lombarde*. Hoepli, Milano, 418 pp.

De Sitter L.U. and De Sitter-Koomans C.M. (1949) Geology of the Bergamasc Alps, Lombardia, Italy. *Leidse Geologische Mededelingen*, **14**, 1-257.

Di Colbertaldo D. (1967) *Giacimenti minerari*. CEDAM, Milano, 383 pp.

De Capitani L. (1982) Contributo alla conoscenza dei plutoni sudalpini: le masse intrusive della Val Biandino (Como). *Rendiconti Società Italiana di Mineralogia e Petrologia*, **38**, 109-118.

De Capitani L. and Liborio G. (1988) Trace element abundance in the Val Biandino Pluton (Southern Alps, Italy). *Memorie della Società di Scienze Geologiche*, **40**, 99-110.

https://doi.org/10.1180/mgm.2024.3 Published online by Cambridge University Press

De Capitani L., Delitala M.C., Liborio G., Mottana A., Nicoletti M. and Petrucciani C. (1988) K–Ar dating of the Val Biandino Plutonic Complex (Orobic Alps, Italy). *Memorie della Società di Scienze Geologiche,* **40**, 285-294.

Deditius A., Utsunomiya S., Ewing R.C. and Kesler S.E. (2009) Nanoscale "liquid" inclusions of As-Fe-S in arsenian pyrite. *American Mineralogist*, **94**, 394.

Deditius A.P., Reich M., Kesler S.E., Utsunomiya S.,. Chryssoulis S.L, Walshe J. and Ewing R.C. (2014) The coupled geochemistry of Au and As in pyrite from hydrothermal ore deposits. *Geochimica et Cosmochimica Acta*, **140**, 644-670.

~~Dill H. and Kemper E. (1990) Crystallographic and chemical variations during pyritization in the upper Barremian and lower Aptian dark claystones from the Lower Saxonian Basin (NW Germany). *Sedimentology,* **37**, 427-443.~~

Einaudi M., Hedenquist J. and Inan E. (2003) Sulfidation state of fluids in active and extinct hydrothermal systems: Transitions from porphyry to epithermal environments. Pp. 285-313 in: *Volcanic, geothermal, and ore-forming fluids: Rulers and witnesses of processes within the Earth*, (S. Simmons and I. Graham, editors). Society of Economic Geologists Special Pubblication, Colorado.

Frenzel M., Tamino H. and Gutzmer J. (2016) Gallium, germanium, indium, and other trace and minor elements in sphalerite as a function of deposit type — A meta-analysis. *Ore Geology Reviews*, **76**, 52-78.

Froitzheim N., Derks J. F., Walter J. M. and Sciunnach D. (2008) Evolution of an Early Permian extensional detachment fault from synintrusive, mylonitic flow to brittle faulting (Grassi Detachment Fault, Orobic Anticline, southern Alps, Italy). *Geological Society London*, **298**, 69-82.

Gaetani M., Sciunnach D., Bini A. and Rossi S. (2012) *Note illustrative della Carta Geologica d'Italia alla scala 1:50.000, F. 076 Lecco*. Progetto CARG, Regione Lombardia, 227 pp.

Genna D. and Gaboury D. (2015) Deciphering the hydrothermal evolution of a VMS system by LA-ICP-MS using trace elements in pyrite: An example from the Bracemac-Mcleod deposits, Abitibi, Canada, and Implications for Exploration. *Economic Geology*, **110**, 2087–2108.

https://doi.org/10.1180/mgm.2024.3 Published online by Cambridge University Press

George L.L., Cook N.J. and Ciobanu C.L. (2017) Minor and Trace Elements in Natural Tetrahedrite-Tennantite: Effects on Element Partitioning among Base Metal Sulphides. *Minerals*, **7**, 17-41.

Golyshev S.I., Padalko N.L. and Pechenkin S.A. (1981) Fractionation of stable oxygen and carbon isotopes in carbonate systems. *Geochemistry International*, **18**, 85-99.

Gottesmann W. and Kampe A. (2007) Zn/Cd ratios in calcsilicatehosted sphalerite ores at Tumurtijn-ovoo, Mongolia. Chemie der Erde – *Geochemistry*, **67**, 323–328.

Gottesmann W., Gottesmann B. and Seifert W. (2009) Sphalerite composition and ore genesis at the Tumurtjin-ovoo Fe–Mn–Zn skarn deposit, Mongolia. *Neues Jahrbuch für Mineralogie*, **185**, 249–280.

Guastoni A., Gentile P. and Nestola F. (2015) Aikinite. Cortabbio, Primaluna, Valsassina (LC). *Rivista Mineralogica Italiana*, **39**, 58-61.

Guastoni A., Gentile P., Nestola F. and Possenti L. (2016) Baumstarkite di Prapiazzo, Introbio, Valsassina (LC). *Rivista Mineralogica Italiana*, **50**, 120.

Guastoni A., Gentile P., Nestola F. and Possenti L. (2016) Imiterite di Prapiazzo, Introbio, Valsassina (LC). *Rivista Mineralogica Italiana*, **50**, 120-121.

~~Guy B., Beukes N. and Gutzmer J. (2010) Paleoenvironmental controls on the texture and chemical composition of pyrite from nonconglomeratic sedimentary rocks of the Mesoarchean Witwatersrand Supergroup, South Africa. *South African Journal of Geology*, **113**, 195–228.~~

Hein U.F. (1993) Synmetamorphic Variscan siderite mineralisation of the Rhenish Massif, Central Europe. *Mineralogical Magazine*, **57**, 451–467.

Hellmann A., Cormann A. and Meyer F.M. (2012) Syn-late orogenic vein hosted Co-Ni mineralization in the Siegerland-District of the Rhenish Massif, NW Germany. *Proceedings of European Mineralogical Conference EMC2012*, **1**, 616.

Hoefs J. (2009) *Stable Isotope Geochemistry*. Springer, Berlin, 286 pp.

Horita J. (2014) Oxygen and carbon isotope fractionation in the system dolomite–water–CO2 to elevated temperatures. *Geochimica et Cosmochimica Acta*, **129**, 111-124.

https://doi.org/10.1180/mgm.2024.3 Published online by Cambridge University Press

Large R.R., Danyushevsky L., Hollit C., Maslennikov V., Meffre S., Gilbert S., Bull S., Scott R., Emsbo P., Thomas H., Singh B. and Foster J. (2009) Gold and trace element zonation in pyrite using a laser imaging technique: implications for the timing of gold in orogenic and Carlin-style sediment-hosted deposits. *Economic Geology*, **104**, 635–668.

Laubsher H.P. (1985) Large-scale, thin-skinned thrusting in the southern Alps: Kinematic models. *Geological Society of America Bulletin*, **96**, 710-718.

Li X., Bai L., Yue Z., Pang B. and Wei D. (2021) Mineralization processes involved in the formation of the Jinya Carlin-type Au deposit, northwestern Guangxi, China: Evidence from in situ trace element and S isotope geochemistry of Au-bearing zoned pyrite. *Ore Geology Reviews*, **138**, 104376.

Locchi S., Zanchetta S. and Zanchi A. (2022) Evidence of Early Permian extension during the post-Variscan evolution of the central Southern Alps (N Italy). *International Journal of Earth Sciences*, **111**, 1717-1738.

Longerich H.P., Jackson S.E. and Günther D. (1996) Laser ablation inductively coupled plasma mass spectrometric transient signal data acquisition and analyte concentration calculation. *Journal of Analytical Atomic Spectrometry*, **11**, 899–904.

Kerrich R., Strong D.F., Andrews A.J. and Owsiacki L. (1986) The silver deposits at Cobalt and Gowganda, Ontario. III: Hydrothermal regimes and source reservoirs - evidence from H, O, C and Sr isotopes and fluid inclusions. *Canadian Journal of Earth Sciences*, **23**, 1519-1550.

Kissin S.A. (1988) Nickel-Cobalt-Native Silver (Five-Element) Veins: A Rift related Ore Type. Pp. 268–279 in: *North American Congress on Tectonic Control of Ore Deposits and the Vertical and Horizontal Extent of Ore Systems*, University of Missouri-Rolla.

Kissin S.A. (1992) Five-element (Ni-Co-As-Ag-Bi) veins. *Geoscience Canada*, **19**, 113–124.

Konnunaho J. P., Hanski E., Karinet T. and Lahaye Y. (2018) The petrology and genesis of the Paleoproterozoic mafic intrusion-hosted Co-Cu-Ni deposit at Hietakero, NW Finnish Lapland. *Bulletin of the Geological Society of Finland*, 104-131.

https://doi.org/10.1180/mgm.2024.3 Published online by Cambridge University Press

Kretschmar U. and Scott S.D. (1976) Phase relations involving arsenopyrite in the system Fe-As-S and their application. *Canadian Mineralogist*, **14**, 364-386.

Klünder-Hansen M., Makovicky E. and Karup-Møller S. (2003) Exploratory studies on substitutions in tetrahedrite-tennantite solid solution. Part IV. Substitution of germanium and tin. N*eues Jahrbuch für Mineralogie*, **179**, 43–71.

Koglin N., Frimmel H.F., Lawrie Minter W.E. and Brätz H. (2010) Trace-element characteristics of different pyrite types in Mesoarchean to Paleoproterozoic placer deposits. *Mineralium Deposita*, **45**, 259-280.

Konnunaho J. P., Hanski E., Karinet T. and Lahaye Y. (2018) The petrology and genesis of the Paleoproterozoic mafic intrusion-hosted Co-Cu-Ni deposit at Hietakero, NW Finnish Lapland. *Bulletin of the Geological Society of Finland*, 104-131.

Kreissl S., Gerdes A., Walter B.F., Neumann U., Wenzel T. and Markl G. (2018) Reconstruction of a>200 Ma multi-stage "five element" Bi-Co-Ni-Fe-As-S system in the Penninic Alps, Switzerland. *Ore Geology Reviews*, **95**, 746–788.

Kullerud G. (1953) The FeS-ZnS system, a geological thermometer. *Norsk Geologisk Tidsskrift*, **32**, 62-144.

Maacha L., Lebedev V.I., Saddiqi O., Zouhair M., Elghorfi M., Borissenko A.S. and Pavlova G.G. (2015) *Arsenide Deposits of the Bou Azzer Ore District ((Anti-Atlas Matallogenic Province) and their Economic Outlook*. TuvIENR SB RAS Monography, Yarmolyuk, 66 pp.

Markl G., Burish M. and Neumann U. (2016) Natural fracking and the genesis of five-element veins. *Mineralium Deposita*, **51**, 703–712.

Marshall D.D., Diamond L.W., and Skippen G.B. (1993) Silver transport and deposition at Cobalt, Ontario, Canada; fluid inclusion evidence. *Economic Geology,* **88**, 837–854.

Martin S., Toffolo L., Moroni M., Montorfano C., Secco L., Agnini P., Nimis P. and Tumiati S. (2017) Siderite deposits in northern Italy: Early Permian to Early Triassic hydrothermalism in the Southern Alps. *Lithos*, **285**, 276-295.

https://doi.org/10.1180/mgm.2024.3 Published online by Cambridge University Press

~~Maslennikov V.V., Maslennikov S.P., Large R.R. and Danyushevsky L.V. (2009) Study of Trace Element Zonation in vent Chimneys from the Silurian Yaman-Kasy Volcanic-Hosted Massive Sulfide Deposit (Southern Urals, Russia) Using Laser Ablation-Inductively Coupled Plasma Mass Spectrometry (LA-ICPMS). *Economic Geology*, **104**, 1111-1141.~~

Matthews A. and Katz A. (1977) Oxygen isotope fractionation during the dolomitization of calcium carbonate. *Geochimica et Cosmochimica Acta*, **41**, 1431-1438.

Mondillo N., Herrington R., Boyce A.J., Wilkinson C., Santoro L. and Rumsey M. (2018) Critical elements in non-sulfide Zn deposits: a reanalysis of the Kabwe Zn-Pb ores (central Zambia). *Mineralogical Magazine*, **82**, 89-114.

Moroni M., Rossetti P., Naitza S., Magnani L., Ruggieri G., Aquino A., Tartarotti P., Franklin A., Ferrari E., and Castelli D. (2019a) Factors controlling hydrothermal nickel and cobalt mineralization - some suggestions from historical ore deposits in Italy. *Minerals*, **9**, 429.

Moroni M., Naitza S., Ruggieri G., Aquino A., Costagliola P., De Giudici G., Caruso S., Ferrari E., Fiorentini M.E. and Lattanzi P. (2019b) The Pb–Zn–Ag vein system at Montevecchio-Ingurtosu, southwestern Sardinia, Italy: A summary of previous knowledge and new mineralogical, fluid inclusion and isotopic data. *Ore Geology Reviews*, **115**, 103194.

Muchez Ph., Heijlen W., Banks D., Blundell D., Boni M. and Grandia F. (2005) Extensional tectonics and the timing and formation of basin-hosted deposits in Europe. *Ore Geology Reviews*, **27**, 241–267.

Ohmoto H. and Rye R.O. (1979) Isotopes of sulfur and carbon. Pp. 509-567 in: *Geochemistry of Hydrothermal Ore Deposits* (H. L. Barnes, editor). John Wiley & Sons, New Jersey.

Ostendorf J., Henjes-Kunst F., Seifert T. and Gutzmer J. (2019) Age and genesis of polymetallic veins in the Freiberg district, Erzgebirge, Germany: constraints from radiogenic isotopes. *Mineralium Deposita*, **54**, 217-236.

Pasquaré G. (1967) Analisi geologico–strutturale del complesso intrusivo di Val Biandino (Alpi Orobie occidentali). *Memorie della Società Geologica Italiana*, **6**, 343–357.

https://doi.org/10.1180/mgm.2024.3 Published online by Cambridge University Press

Paul D., Skrzypek G. and Fórizs I. (2007) Normalization of measured stable isotopic compositions to isotope reference scales – A review. *Rapid Communications in Mass Spectrometry*, **21**, 3006–3014.

Pohl F., Froitzheim N., Obermüller G., Tomaschek F., Schröder O., Nagel T. J., Sciunnach D. and Heuser A. (2018) Kinematics and Age of Syn-Intrusive Detachment Faulting in the Southern Alps: Evidence for Early Permian Crustal Extension and Implications for the Pangea A Versus B Controversy. *Tectonics*, **37**, 3668-3689.

Price B.G. (1972) *Minor elements in pyrites from the Smithers Map area, B.C. and exploration applications of minor elements studies.* PhD dissertation, University of British Columbia, Canada.

Qian X. (1987) Trace elements in galena and sphalerite and their geochemical significance in distinguishing the genetic types of Pb–Zn ore deposits. *Chinese Journal of Geochemistry*, **6**, 177–190.

Rajabpour S., Behzadi M., Jiang S.Y., Rasa I., Lehmann B. and Ma Y. (2017) Sulfide chemistry and sulfur isotope characteristics of the Cenozoic volcanic-hosted Kuh-Pang copper deposit, Saveh county, northwestern central Iran. *Ore Geology Reviews*, **86** , 563-583.

Ramdohr P. (1975) Der Silberkobalterzgang mit Kupfererzen vom Wingertsberg bei Nieder-Ramstadt im Odenwald. *Aufschluss*, **27**, 237–243.

Reich M., Kesler S.E., Utsunomiya S., Palenik C.S., Chryssoulis S.L. and Ewing R.C. (2005) Solubility of gold in arsenian pyrite. *Geochimica et Cosmochimica Acta*, **69**, 2781-2796.

Reich M., Deditius A., Chryssoulis S., Li J.W., Ma C.Q., Parada M.A., Barra F. and Mittermayr F. (2013) Pyrite as a record of hydrothermal fluid evolution in a porphyry copper system: a SIMS/EMPA trace element study. *Geochimica et Cosmochimica Acta*, **104**, 42-62.

Robinson B.W. and Badham J.P.N. (1974) Stable isotope geochemistry and the origin of the Great Bear Lake silver deposits, Northwest Territories, Canada. *Canadian Journal of Earth Sciences*, **11**, 698-711.

Rodeghiero F., Jadoul F., Vailati G. and Venerardi I. (1987) Dati preliminari sulle mineralizzazioni a Pb–Zn dell'area tra Mandello e Ballabio (Lombardia Centrale). *Memorie della Società Geologica Italiana*, **32**, 133–150.

https://doi.org/10.1180/mgm.2024.3 Published online by Cambridge University Press

Schwartz M.O. (2000) Cadmium in zinc deposits: economic geology of a polluting element. *International Geology Review*, **42**, 445–469.

Sciunnach D (2001) Early Permian Palaeofaults at the western boundary of the Collio Basin (Valsassina, Lombardy). *Natura Bresciana*, **25**, 37–43.

~~Scott R., Meffre S., Woodhead J., Gilbert S.E., Berry R.F. and Emsbo P. (2009) Development of framboidal pyrite during diagenesis, low-grade regional metamorphism and hydrothermal alteration. *Economic Geology*, **104**, 1143-1168.~~

Segalstad T.V., Johansen H. and Ohmoto H. (1986) Geochemistry of hydrothermal processes at the Kongsberg silver deposit, southern Norway. *Terra Cognita*, **6**, 511-555.

Seifert T. and Sandmann D. (2006) Mineralogy and geochemistry of indium-bearing polymetallic vein-type deposits: Implications for host minerals from the Freiberg district, Eastern Erzgebirge, Germany. *Ore Geology Reviews*, **28**, 1-31.

Sharp Z.D., Essene E.J. and Kelly W.C. (1985) A re-examination of the arsenopyrite geothermometer: pressure considerations and applications to natural assemblages. *Canadian Mineralogist,* **23**, 517-534.

Sheppard S. M. F. and Taylor H. P. (1977) Hydrogen and Oxygen Isotope Evidence for the Origins of Water in the Boulder Batholith and the Butte Ore Deposits, Montana. *Economic Geology*, **69**, 926-946.

Siletto G.B., Spalla M.I., Tunesi A., Lardeaux J.M. and Colombo A. (1993) Pre–Alpine Structural and Metamorphic Histories in the Orobic Southern Alps, Italy. *Pre-Mesozoic Geology in the Alps*, 585–598.

Schmidt Mumm A. and Wolfgramm M. (2004) Fluid systems and mineralization in the north German and Polish basin. *Geofluids*, **4**, 315-328.

Servida D., Moroni M., Ravagnani D., Rodeghiero F., Venerandi I., De Capitani L. and Grieco G. (2010) Phreatic sulphide bearing quartz breccias between crystalline basement and Collio formation (Southern Alps, Italy). *Italian Journal of Geosciences*, **129**, 223-236.

https://doi.org/10.1180/mgm.2024.3 Published online by Cambridge University Press

Staude S., Werner W., Mordhorst T., Wemmer K., Jacob D.E. and Markl G. (2012) Multi-stage Ag–Bi–Co–Ni–U and Cu–Bi vein mineralization at Wittichen, Schwarzwald, SW Germany: geological setting, ore mineralogy, and fluid evolution. *Mineralium Deposita*, **47**, 251–276.

Thöni M., Mottana A., Delitala M.C., De Capitani L. and Liborio G. (1993) The Val Biandino composite pluton: A late Hercynian intrusion into the South–Alpine metamorphic basement of the Alps (Italy). *Neues Jahrbuch für Mineralogie*, **12**, 545–554.

Tizzoni M. (1998) *Il comprensorio minerario e metallurgico valsassinese*. Monografie Museo Civico Lecco, Lecco, 447 pp.

Tizzoni M., Invernizzi P. and Lambrugo M. (2015) *Memorie dal sottosuolo, per una storia mineraria della Valsassina*. Bellavite Editore, Missaglia, 183 pp.

Vergani F. (2019) *Le mineralizzazioni filoniane a solfuri della Valsassina: studio giacimentologico preliminare.* Master thesis dissertation, University of Milano, Italy.

Vergani F., Gentile P., Guastoni A., and Possenti L. (2020) La mineralizzazione ad arseniati e i minerali di antimonio di Passo Camisolo, Introbio (LC) e Valtorta (BG). *Rivista Mineralogica Italiana*, **44**, 44-62.

Vergani F. (2022) A preliminary petrographic and LA-ICP-MS trace elements study of the iron sulfide-rich deposits of Lombard Southern Alps: evidences of a hydrothermal origin? *Periodico di Mineralogia,* **91**, 201-224.

Wang C.M., Yang L., Bagas L., Evans N.J., Chen J. and Du B. (2018) Mineralization processes at the giant Jinding Zn-Pb deposit, Lanping Basin, Sanjiang Tethys Orogen: evidence from in situ trace element analysis of pyrite and marcasite. *Geological Journal*, **53**, 1279-1294.

Warr L.N. (2021) IMA–CNMNC approved mineral symbols. *Mineralogical Magazine*, **85**, 291 - 320.

Ye L., Cook N.J., Ciobanu C.L., Liu Y.P., Zhang Q., Liu T.G., Gao W., Yang Y.L. and Danyushevskiy L. (2011) Trace and minor elements in sphalerite from base metal deposits in South China: a LA-ICPMS study. *Ore Geology Review*, **39**, 188-217.

https://doi.org/10.1180/mgm.2024.3 Published online by Cambridge University Press

Zanchetta, S., Malusà, M. G. and Zanchi, A. (2015) Precollisional development and Cenozoic evolution of the Southalpine retrobelt (European Alps). *Lithosphere*, **7**, 662-681.

Zanchetta S., Locchi S., Carminati G., Mancuso M., Montemagni C. and Zanchi A. (2022) Metasomatism by Boron-Rich Fluids along Permian Low-Angle Normal Faults (Central Southern Alps, N Italy). *Minerals*, **12**, 404.

Zheng Y.F. (1999) Oxygen isotope fractionation in carbonate and sulfate minerals. *Geochemical Journal*, **33**, 2, 109-126.

https://doi.org/10.1180/mgm.2024.3 Published online by Cambridge University Press

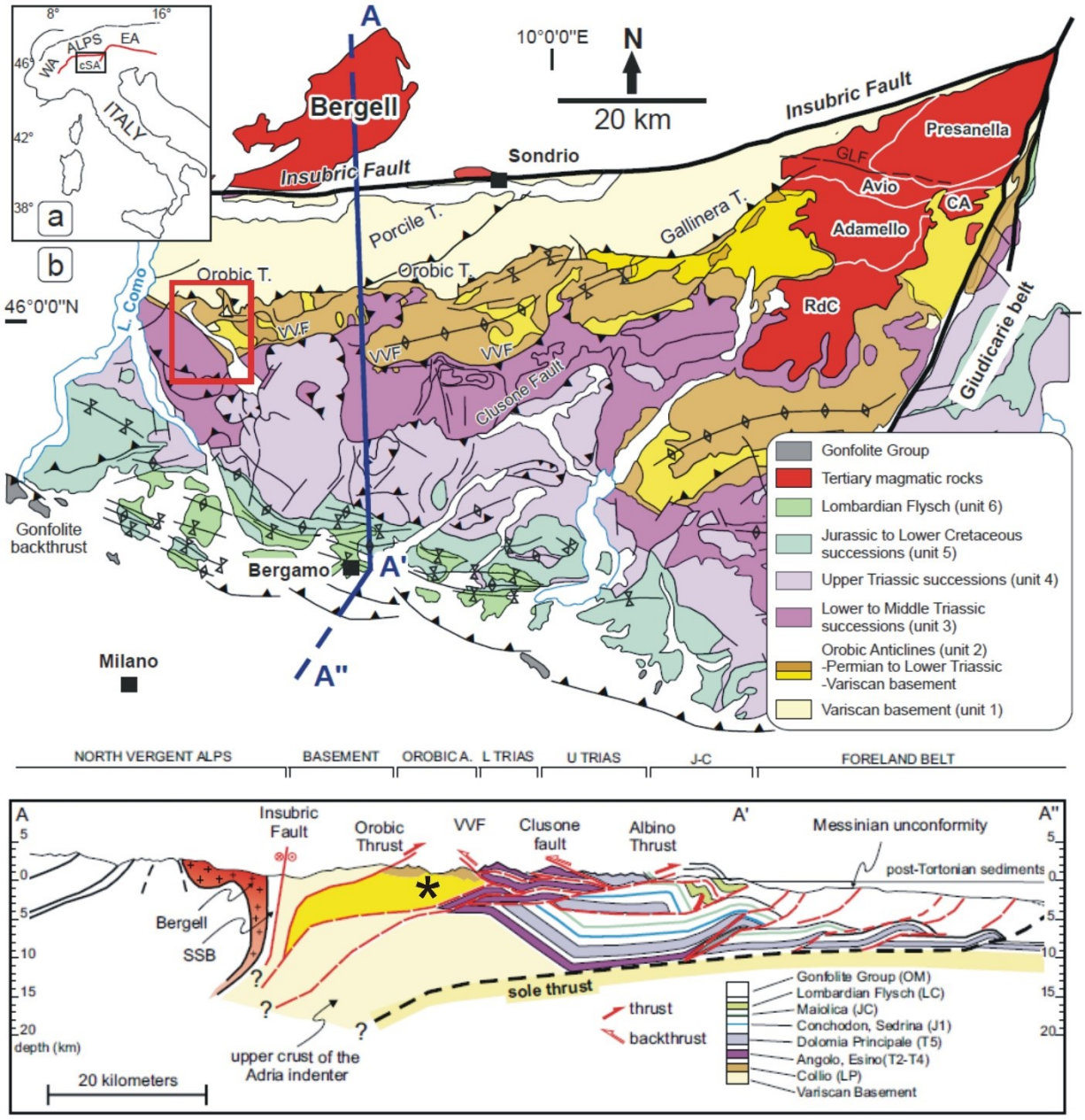

Fig 1. Geological sketch map of the South-alpine domain in Lombardy. The Valsassina Valley area is inscribed in the red rectangle. This valley is characterized by two main geological areas, separated by the Valtorta Fault (VVF). In the section, the black asterisk indicates the Orobic Basement. Reproduced from Zanchetta et al. (2015).

https://doi.org/10.1180/mgm.2024.3 Published online by Cambridge University Press

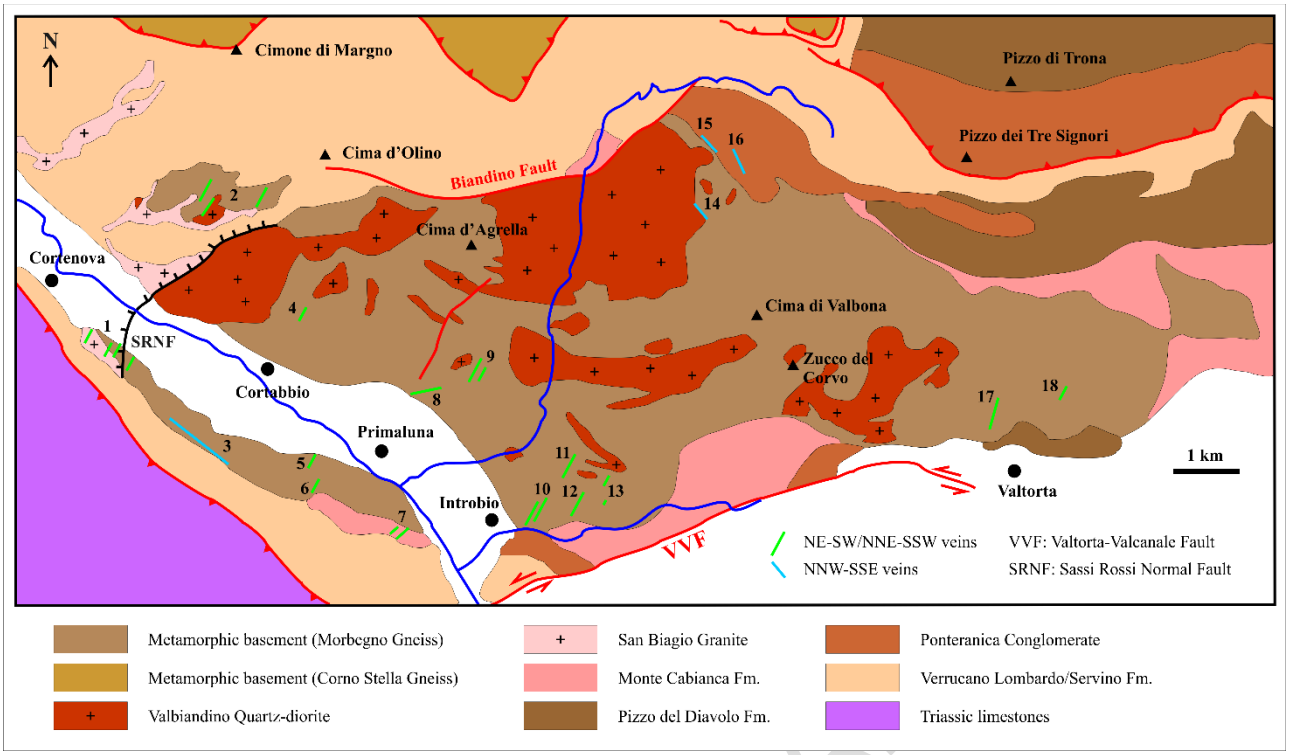

Fig 2. Simplified geological map showing the main lithologies, the position of the intrusive masses and the principal mining areas of Valsassina. Most of the orebodies are hosted inside the metamorphic basement or in proximity of the contacts with the intrusive masses, whereas the Camisolo and Pra Piazzo lodes are hosted by Permian volcano-clastic rocks.

https://doi.org/10.1180/mgm.2024.3 Published online by Cambridge University Press

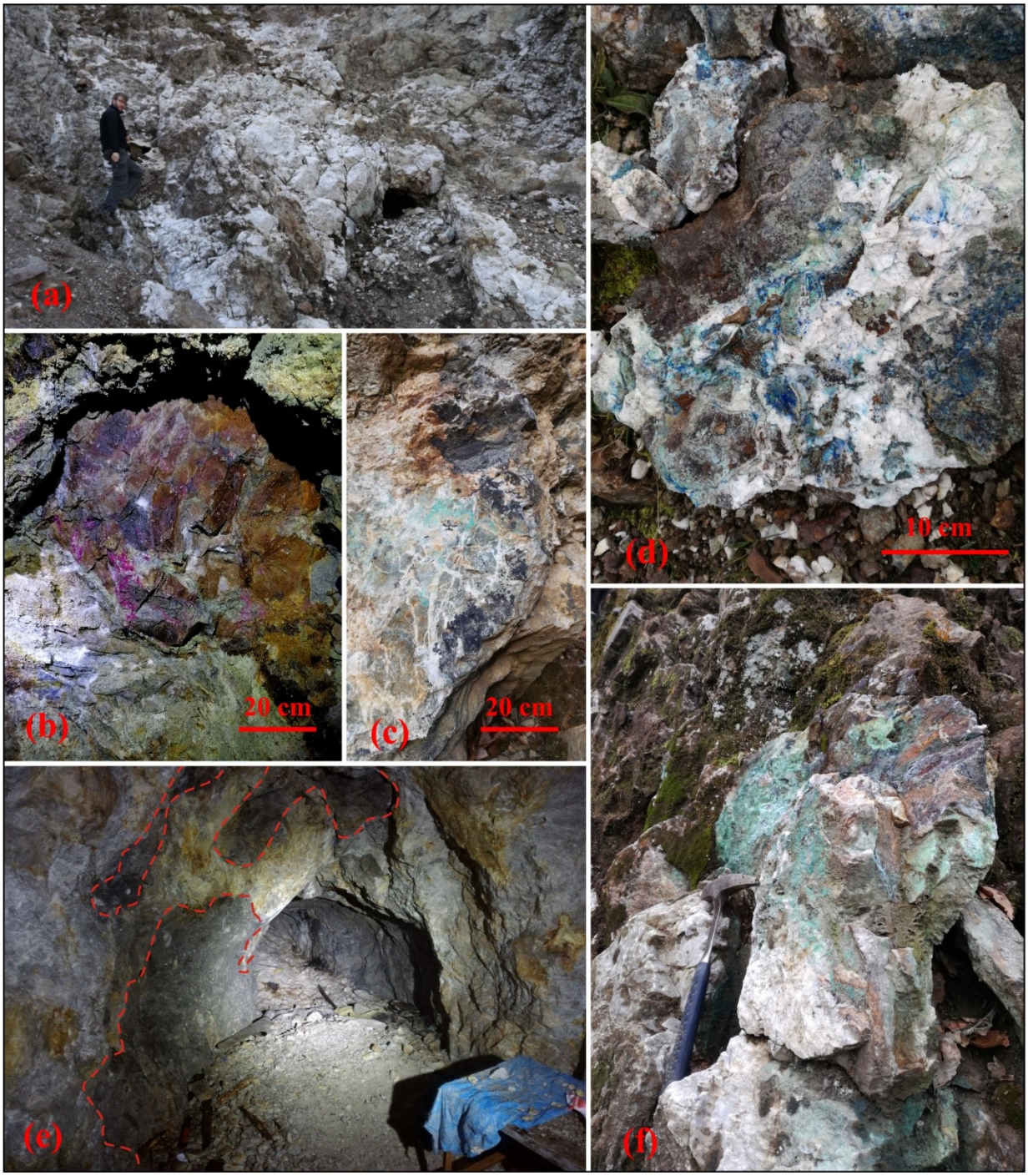

Fig 3. Field configurations of the mineralization in the veins of the Valsassina mining district: (a) outcrop of the big Camisolo lode in the northern part of the mining area, between Santa Barbara and Lina levels; (b) Ni-Co mineralization in carbonate gangue, with minor Co-bearing secondary phases (Cortabbio mines); (c) stockwork quartz veinlets associated with a broad malachite crust (Valtorta lode); (d) baryte vein up to 20 cm thick, hosted in volcanic rocks, that includes several host rock fragments and that is covered by various Cu minerals due to tetrahedrite oxidation (Camisolo mine area); (e) view of the mineralization in the deeper part

https://doi.org/10.1180/mgm.2024.3 Published online by Cambridge University Press

of the Pra Piazzo mine, where the lode consists mainly of quartz and dolomite with minor galena (white and yellowish part of the rocks, underlined by the red dotted line); (f) Cortabbio mine open works, contact between the chalcopyrite-bearing baryte ore body and the host schists.

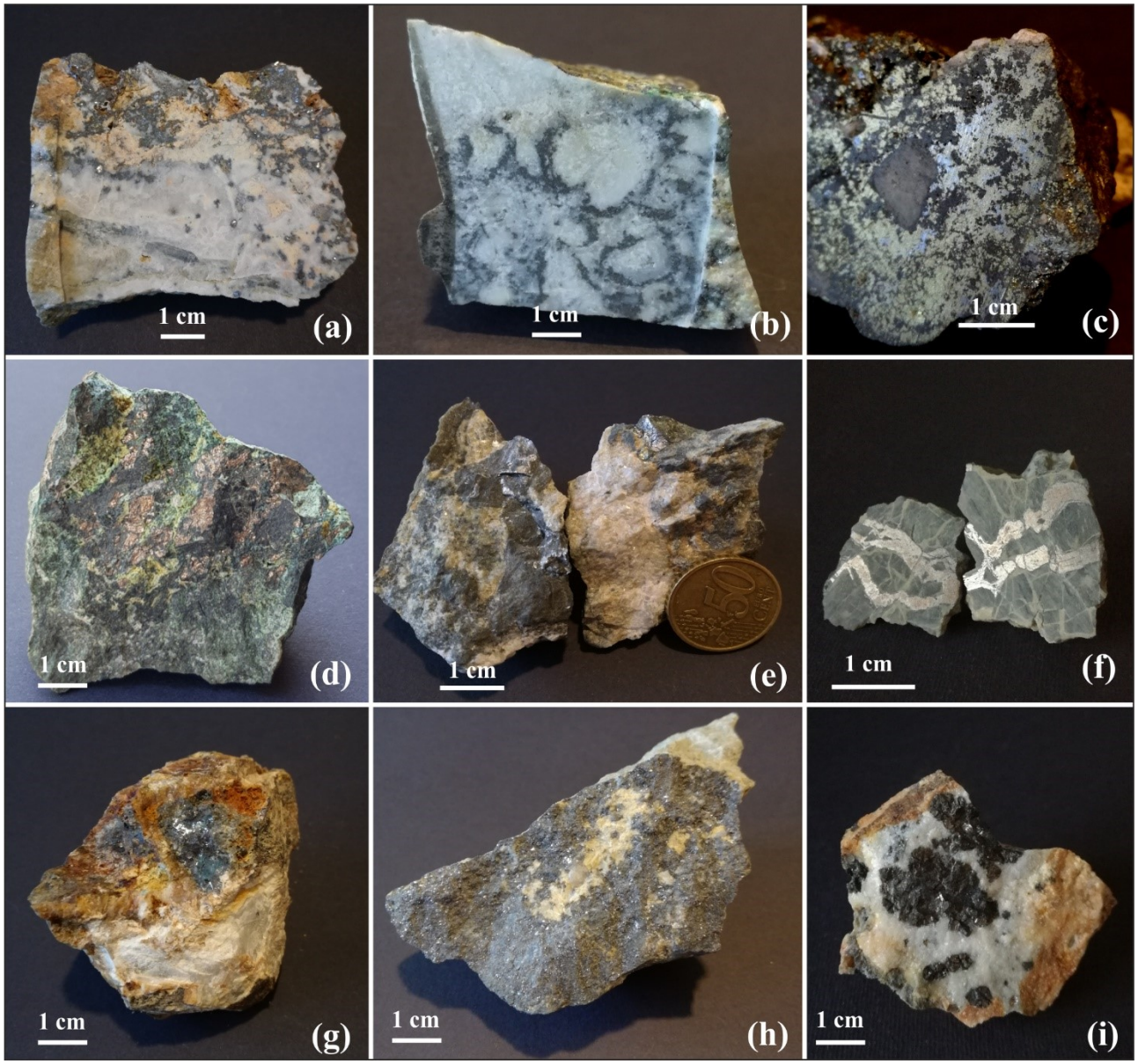

Fig 4. Macroscopic textures of the mineralization in the veins of the Valsassina mining district: (a) galena disseminations within a quartz (white) and siderite (yellowish) gangue, Valbona mine; (b) quartz rich sample with abundant tetrahedrite from Camisolo mine; (c) detail of a cut semi-massive ore sample from Cortabbio mines, Virginia open pit: chalcopyrite rich of inclusions, apparently of major tetrahedrite s.s.; (d) massive Ni-Co-Fe arsenides nodules with abundant annabergite. Cortabbio mines; (e) nodules of Ni-Co-Fe arsenides sealed in carbonate gangue from Cortabbio mines; (f) Ni-Co-Fe arsenides veins that cross the host schist,

https://doi.org/10.1180/mgm.2024.3 Published online by Cambridge University Press

associated with hydrothermal carbonate veinlets, Cortabbio mines; (g) galena nodules with limonite (due to siderite and pyrite oxidation) in baryte and (minor) quartz gangue, Ombrega lead prospect; (h) galena-rich sample in carbonate (dolomite) gangue from Pra Piazzo mine; (i) Dark sphalerite nodules in quartz gangue from Costa Alta mine (Valtorta lode).

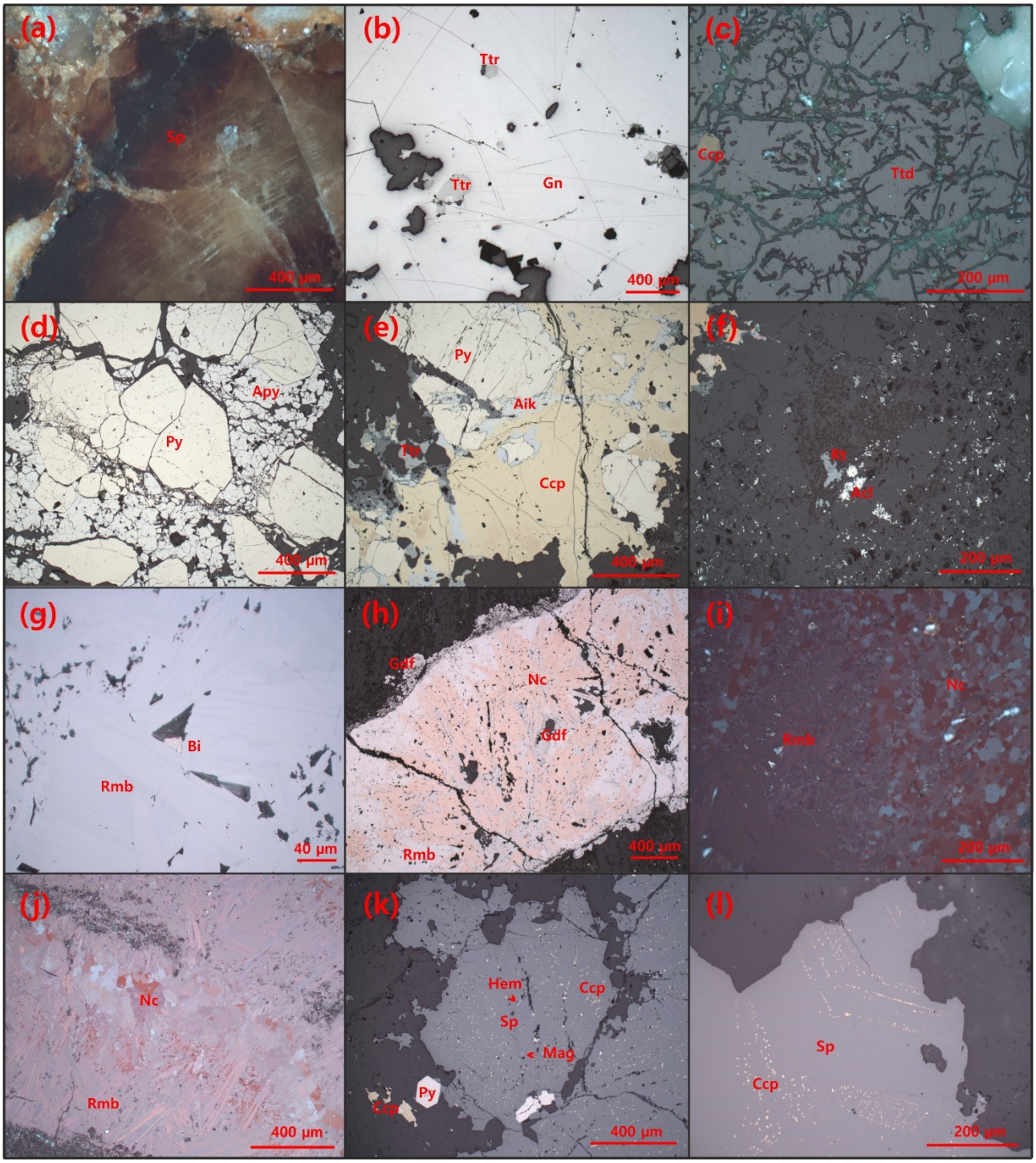

Fig 5. Microscopic features of ore minerals in the veins of the Valsassina mining district (reflected light microscopy): (a) a large sphalerite crystal displaying optical zoning with a homogeneously light coloured,

https://doi.org/10.1180/mgm.2024.3 Published online by Cambridge University Press

transparent interior surrounded by a dark rim, Valbona mine; (b) amoeboid inclusions of tetrahedrite (grey) in galena (white), Camisolo mine; (c) cuproroméite with dark green internal reflections in tetrahedrite fractures. A yellow grain of chalcopyrite is also observable, Camisolo mine (crossed Nicols); (d) euhedral yellowish white, subhedral pyrite crystals surrounded by interstitial arsenopyrite with marked brecciated texture, Valbona mine; (e) light grey inclusions of galena and Ag-Bi bearing sulfides and sulfosalts in chalcopyrite (associated to pyrite and terahedrite on the left), Cortabbio mines; (f) small alloclasite and glaucot white crystals in quartz gangue; some rutile grains (grey) are also observable (Cortabbio mines); (g) massive Ni-Co-Fe arsenides in a veinlet from the Cortabbio mines. In the core of the aggregate, pink nickeline rosettes are overgrown (and partly replaced) by aggregates of greyish white, lamellar rammelsbergite crystals. Gersdorffite-cobaltite crusts (grey) grow on the external surface of the arsenide aggregate and also penetrate it, replacing both rammelsbergite and nickeline; (h) native bismuth (yellowish) associated to rammelsbergite acicular crystals, Cortabbio mines. (i)(j): crossed-Nicols microphotos of nickeline rosettes, showing a peculiar mosaic texture, and, nearby, the aggregates of acicular crystals of rammelsbergite (Cortabbio mines); (k) sphalerite rich in tiny chalcopyrite inclusions associated with minor hematite and magnetite (asterisks), Valtorta lode; (l) sphalerite displaying chalcopyrite disease-like texture along thin bands in the Val Rossiga vein. All mineral name abbreviations are from Warr (2021).

https://doi.org/10.1180/mgm.2024.3 Published online by Cambridge University Press

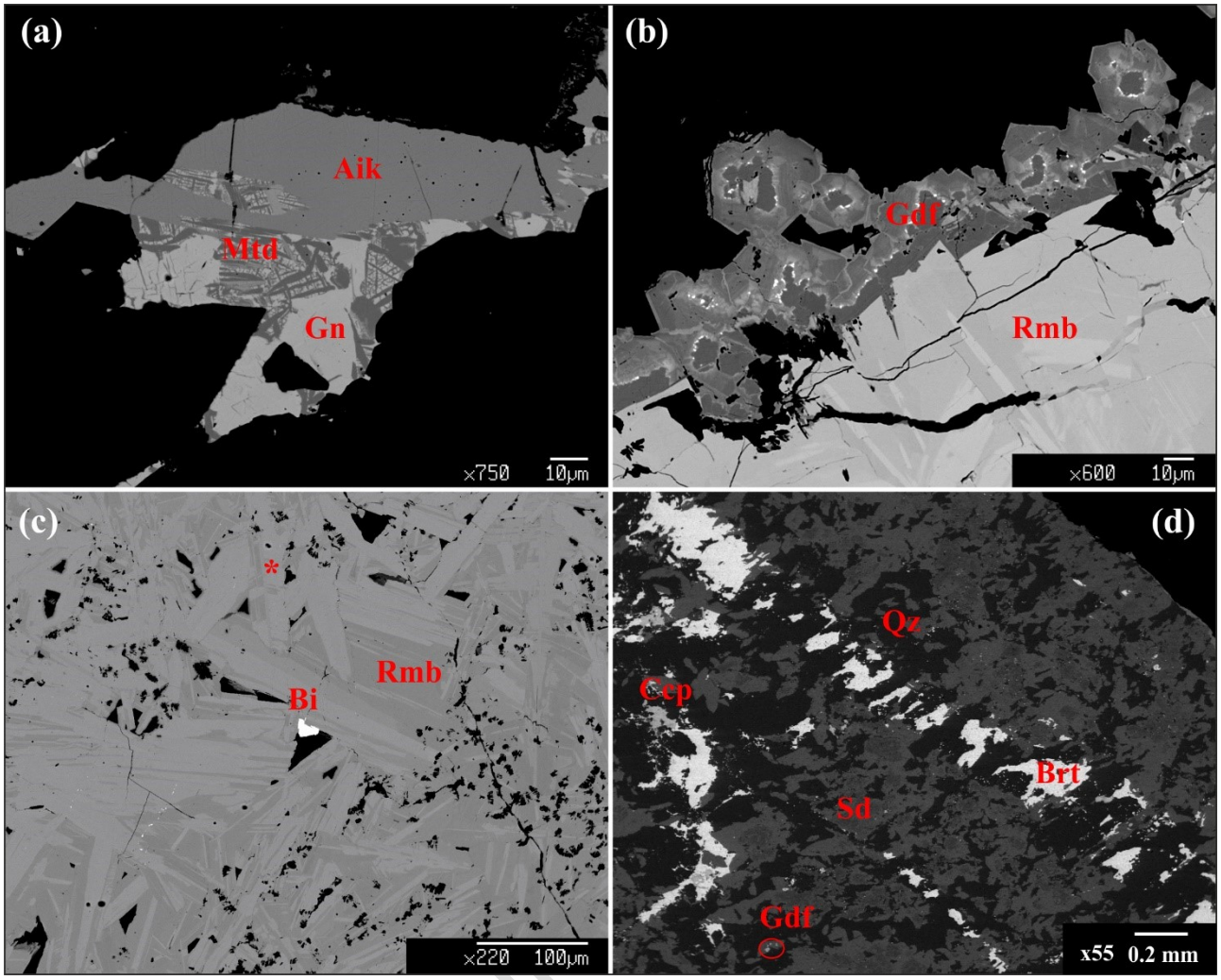

Fig 6. Microtextural (and microchemical) features of ore mineral species in the veins of the Valsassina mining district observed in SEM backscattered imaging: (a) exsolution lamellae of matildite (dark grey) in galena (light grey), associated with aikinite (mid-grey, upper part of the aggregate) from the Cortabbio mines; (b) crust formed by zoned gersdorffite-cobaltite grains on the external surface of rammelsbergite aggregates (light grey lamellar crystals). Segregations of native-bismuth (white inclusions) are visible in the gersdorffite-cobaltite growth zones (Cortabbio mines); (c) zoned lamellar crystals of rammelbergite associated with an interstitial grain of native bismuth; additional bismuth is also visible, as very small white inclusions, along a thin crack in rammelsbergite, in the lower left part of the image. Cortabbio Mines; (d) baryte-chalcopyrite veinlet evidently cut by siderite and quartz in a Ni-Co-Fe nodule from Cortabbio mines. The siderite is zoned, with a Mg-rich core. Minor gersdorffite crystals are also present mainly in association to siderite.

https://doi.org/10.1180/mgm.2024.3 Published online by Cambridge University Press

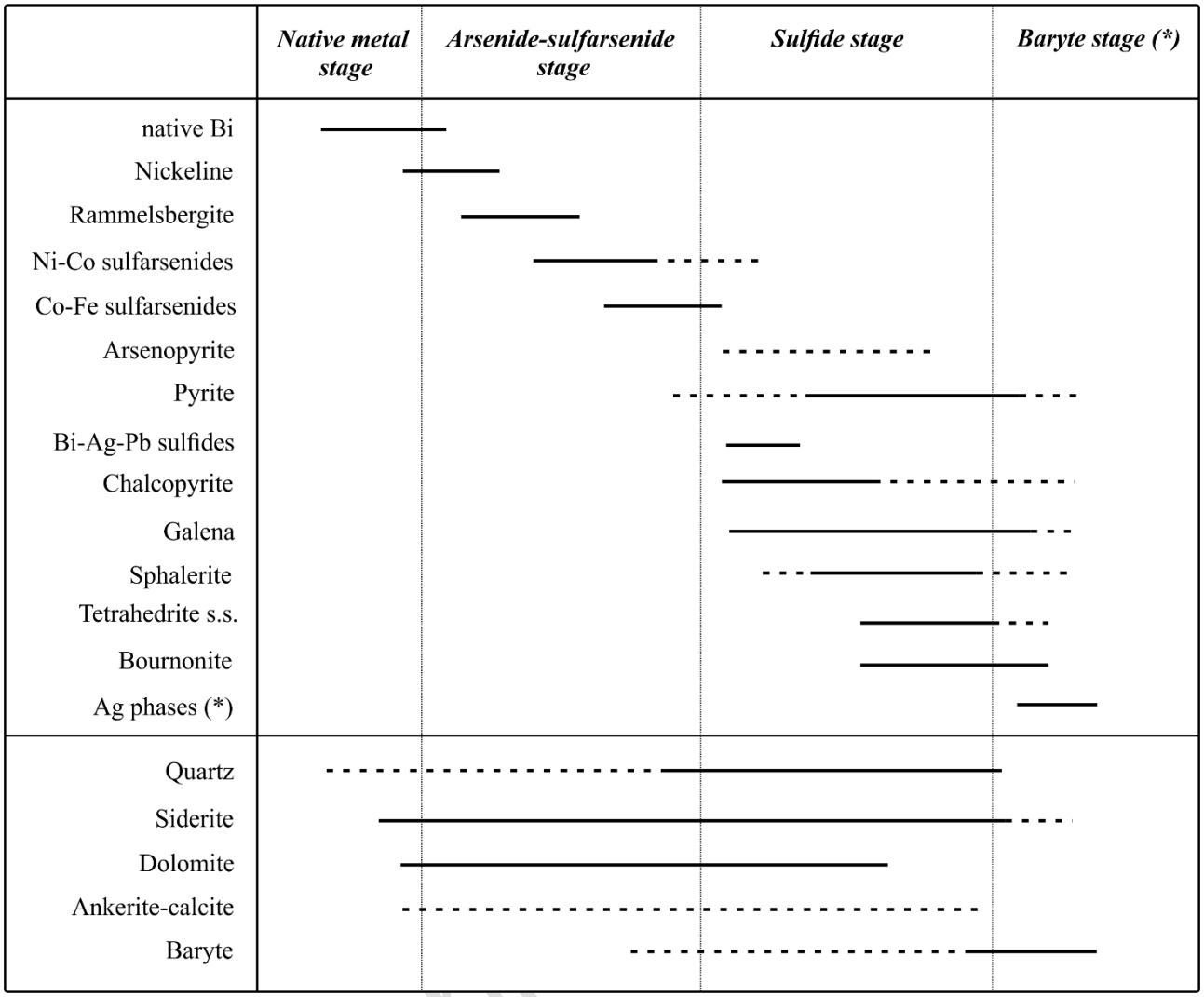

Fig 7. Preliminary paragenetic scheme of the Valsassina veins. In particular, the Ni-Co arsenide/sulfarsenide stage of Cortabbio shows strong analogies with the so-called "five-element veins". Note that Ni-Co minerals are always older than the sulfide.

https://doi.org/10.1180/mgm.2024.3 Published online by Cambridge University Press

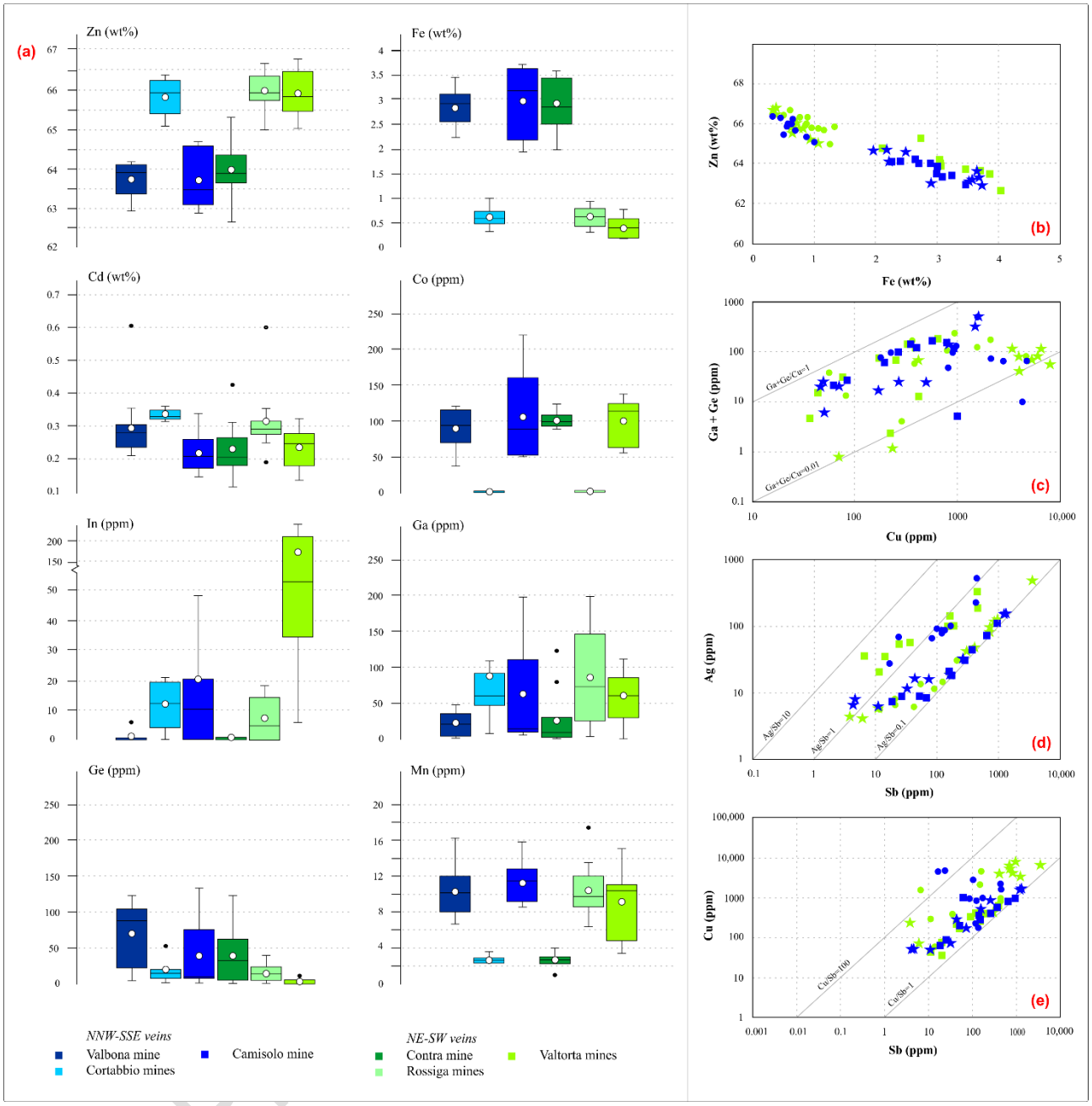

Fig 8. Major, minor and trace element plots of sphalerite: (a) statistical dispersion box-plots of Zn, Fe, Cd, Co, In, Ga, Ge and Mn (for all the boxplots, the colored box contains 50% of the data, the white dot indicates the mean, the horizontal continuous line the median, while the black dots represent the outliers); (b) Zn vs. Fe; (c) Ga + Ge vs. Cu; (d) Ag vs. Sb and (e) Cu vs. Sb. Blue squares: Valbona, blue circles: Cortabbio, blue stars: Camisole, green squares: Valle di Contra, green circles: Val Rossiga, green stars: Valtorta.

https://doi.org/10.1180/mgm.2024.3 Published online by Cambridge University Press

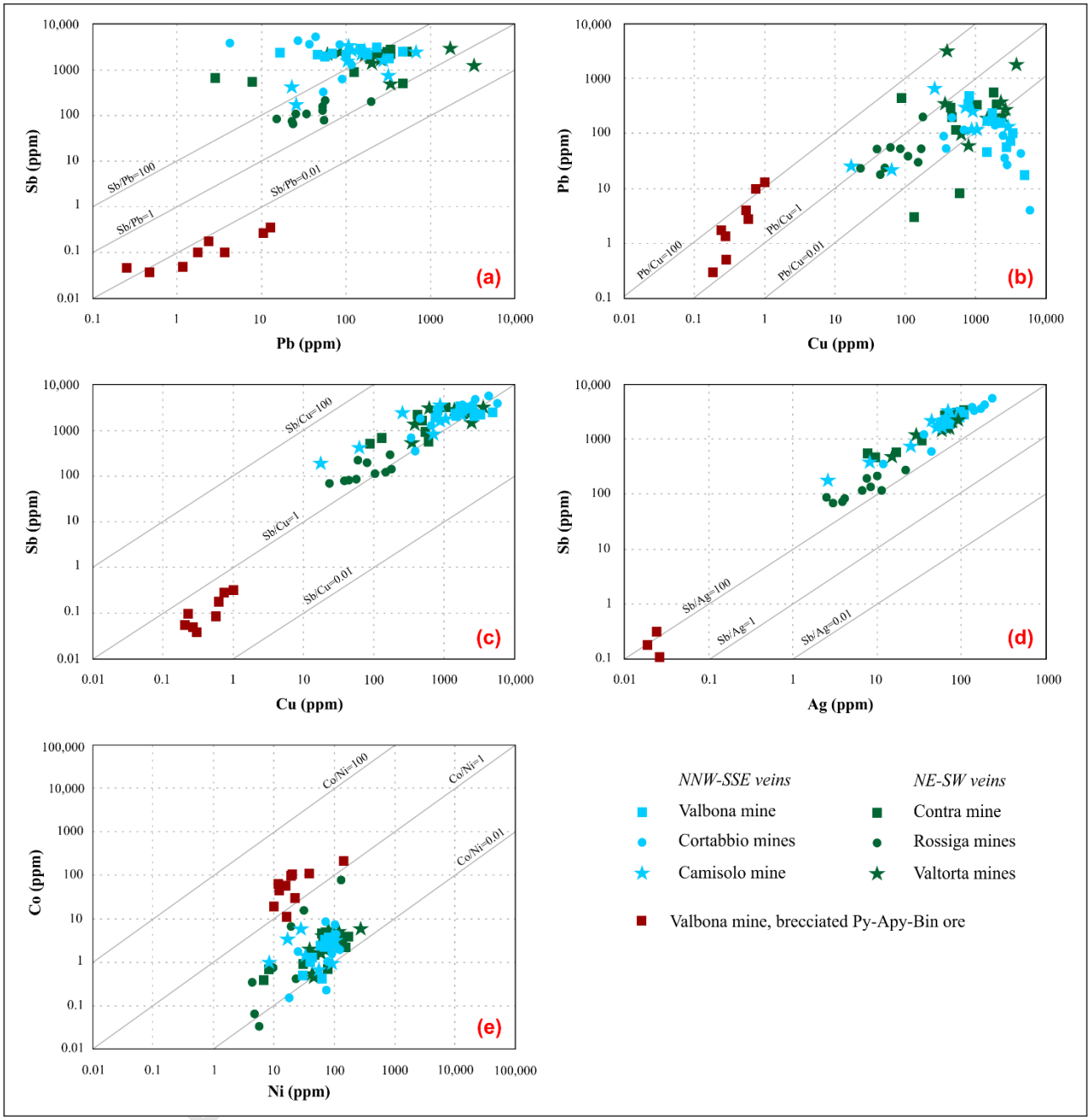

Fig 9. Trace elements binary plots of the pyrite compositional data: (a) Sb vs. Pb; (b) Sb vs Cu; (c) Sb vs. Ag; (d) Sb vs. Cu; (e) Co vs. Ni.

https://doi.org/10.1180/mgm.2024.3 Published online by Cambridge University Press

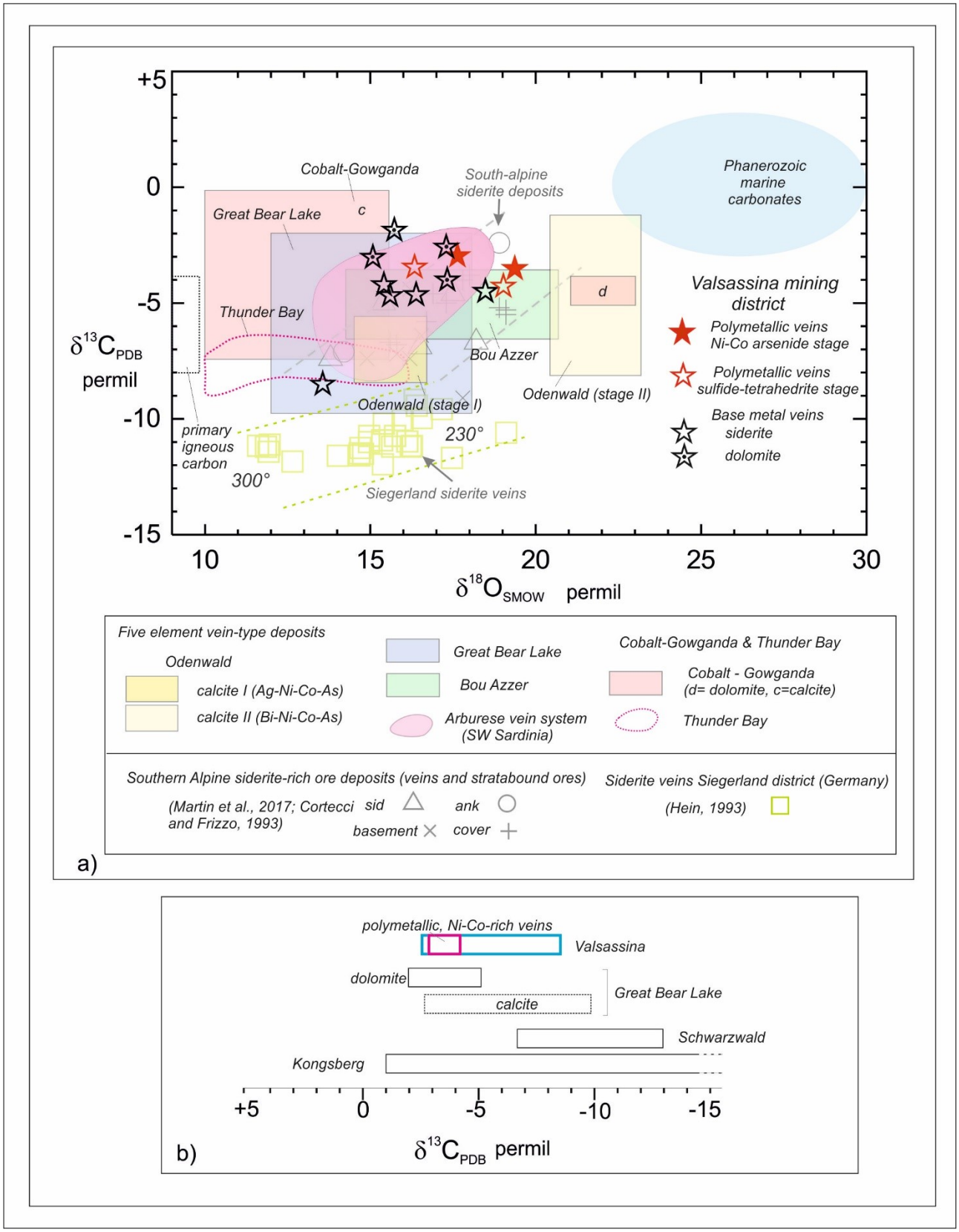

Fig 10. Carbon and oxygen isotope composition of ore-related carbonates in the Valsassina veins: the $\delta^{18}O$ (V-SMOW) and $\delta^{13}C$ (V-PDB) diagram in (a) and the $\delta^{13}C$ (V-PDB)-only plot in (b) display the isotopic signatures

https://doi.org/10.1180/mgm.2024.3 Published online by Cambridge University Press

of siderite and dolomite from the base metal sulfide-rich and polymetallic veins, and compare them with several datasets from worlwide five-element vein-type deposits.

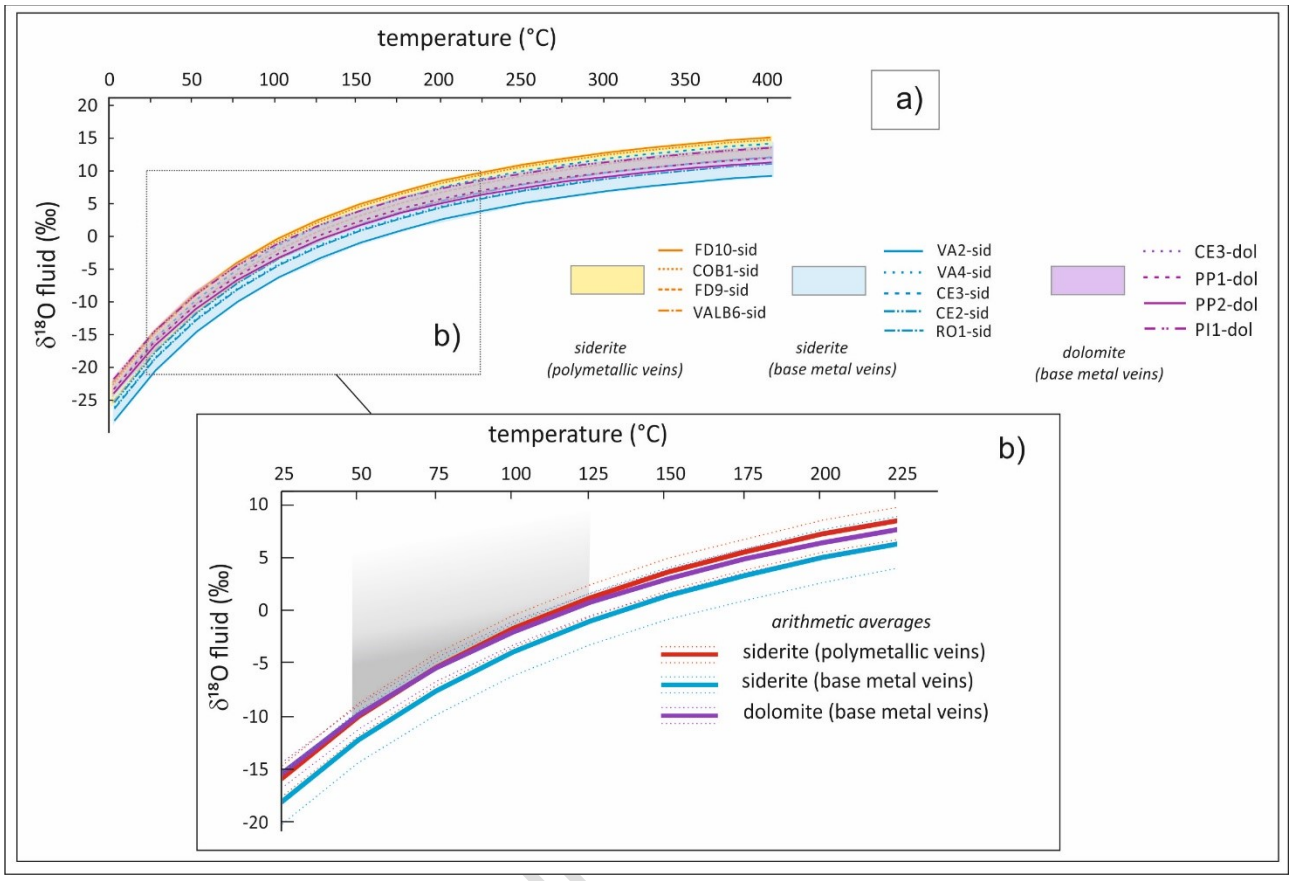

Fig 11. (a) Mineral–fluid fractionation curves based on $\delta^{18}O$‰ V-SMOW of siderite and dolomite in samples from polymetallic veins and from base-metal veins within the Valsassima hydrothermal system. (b) Detail of (a) with the plot of the arithmetic averages of each group of mineral-water fractionation curves.

https://doi.org/10.1180/mgm.2024.3 Published online by Cambridge University Press

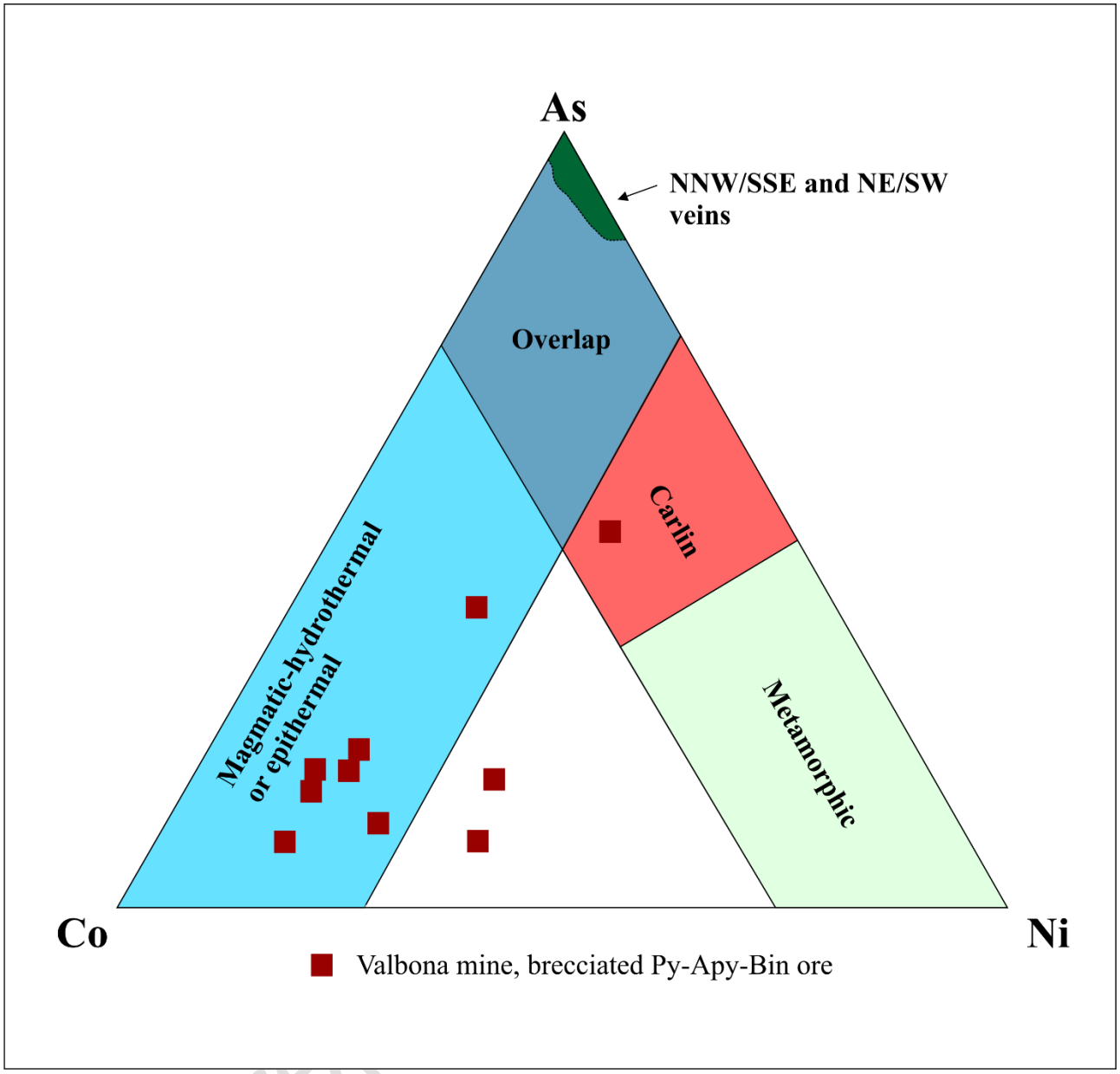

Fig 12. Valsassina pyrite compositions compared to other deposits on a Co–Ni–As projection (modified from Rajabpour et al., 2017). Pyrite from the NNW-SSE and NE-SW vein lies near the As apex, instead the brecciated Valbona pyrite plots shifted toward the Co apex.

https://doi.org/10.1180/mgm.2024.3 Published online by Cambridge University Press

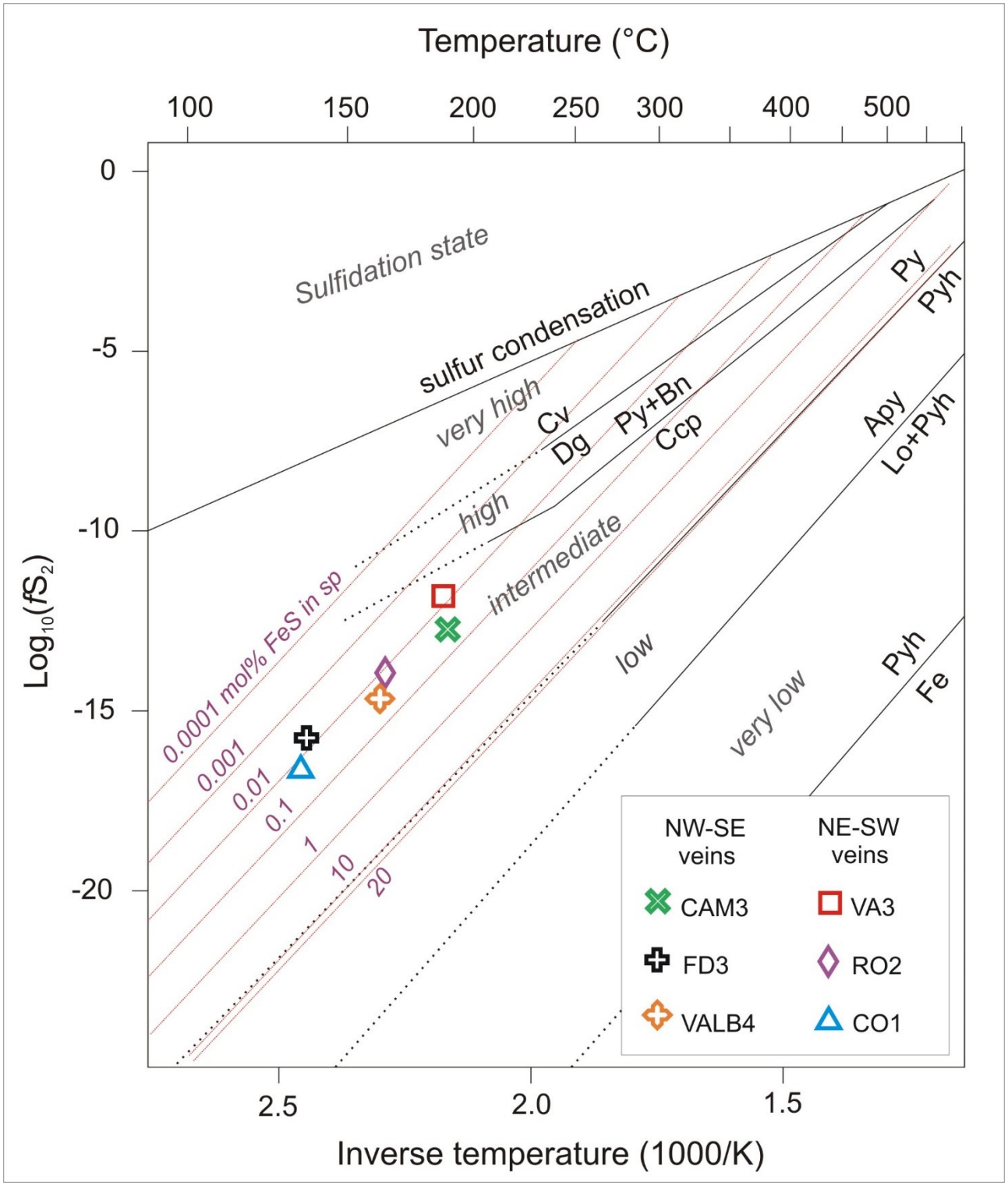

Fig 13. Sulfur fugacity-temperature diagram with mineral reaction lines (black) and isolines of Fe concentrations in sphalerite (red). Sphalerites from the NW-SE veins and from the NE-SW veins are plotted on the basis of their average %FeS molar contents and of their GGIMFis temperatures. Labels: Apy = arsenopyrite, Bn = bornite, Ccp = chalcopyrite, Cv = covellite, Dg = digenite, Fe = native iron, Lo = löllingite, Po = pyrrhotite, Py = pyrite, Sp = sphalerite. Modified after Einaudi et al. (2003).

https://doi.org/10.1180/mgm.2024.3 Published online by Cambridge University Press

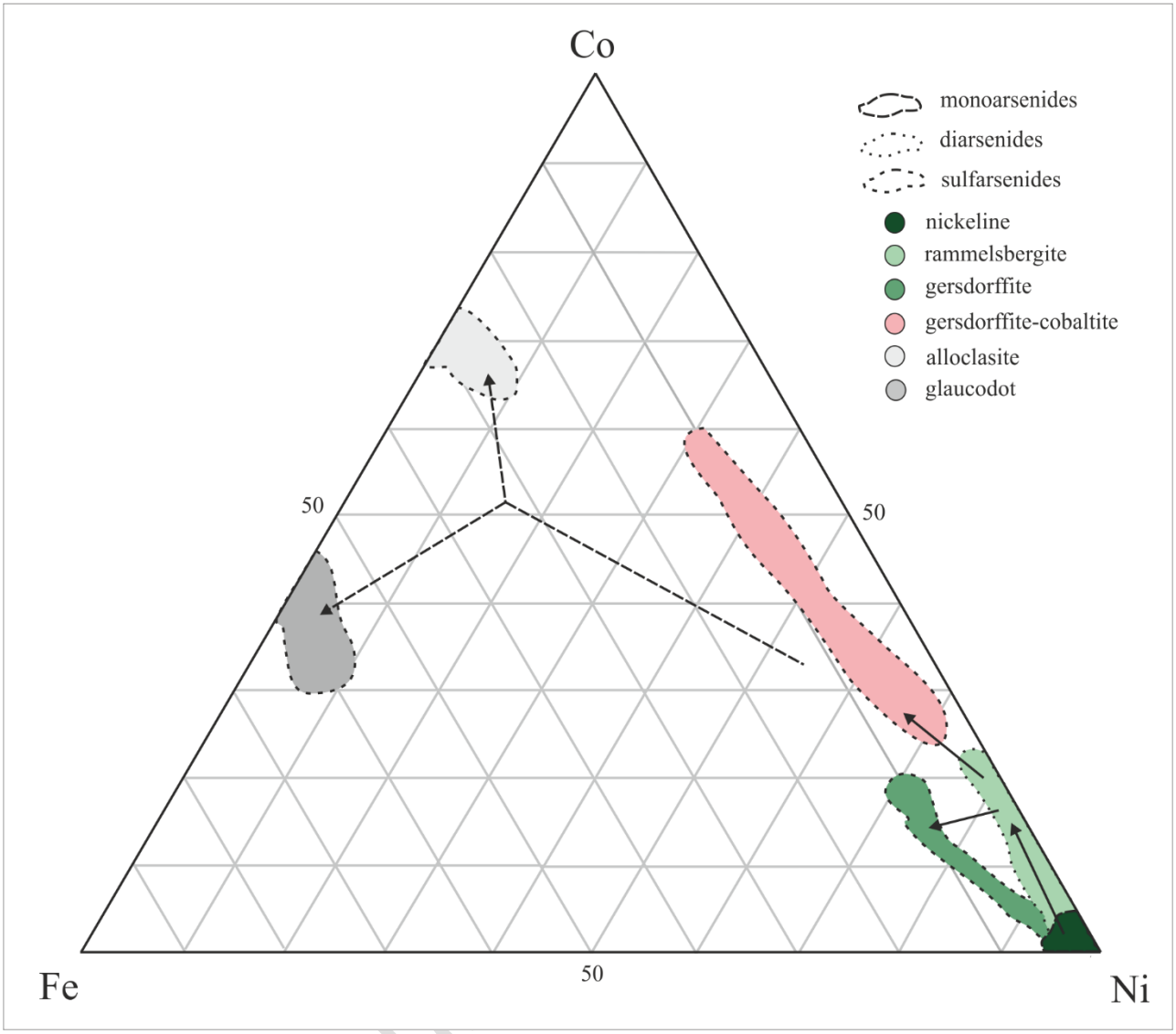

Fig 14. Ternary plot resuming the composition of the Cortabbio Ni-Co-Fe arsenide and sulfarsenides for evaluating the chemical trends in the precipitation sequence of these mineral phases (based on the petrographic observations) and for comparing them with what observed in five-element veins worldwide. The first crystallized phases show Ni-only or Ni-rich compositions (*e.g.* nickeline and, partly, rammelsbergite), whereas the phases deposited subsequently show gradual compositional variations, with moderate and progressive enrichments in Co and then in Co and Fe, coupled with increase in As (from mono- to diarsenide) and then input of sulfur (sulfarsenides).

https://doi.org/10.1180/mgm.2024.3 Published online by Cambridge University Press